nature COMMUNICATIONS

ARTICLE

Received 29 Nov 2013 | Accepted 24 Jun 2014 | Published 1 Sep 2014

DOI: 10.1038/ncomms5485 OPEN

A Cenozoic-style scenario for the end-Ordovician glaciation

Jean-François Ghienne[1], André Desrochers[2], Thijs R.A. Vandenbroucke[3], Aicha Achab[4], Esther Asselin[5], Marie-Pierre Dabard[6], Claude Farley[2], Alfredo Loi[7], Florentin Paris[6], Steven Wickson[2] & Jan Veizer[2]

The end-Ordovician was an enigmatic interval in the Phanerozoic, known for massive glaciation potentially at elevated CO_2 levels, biogeochemical cycle disruptions recorded as large isotope anomalies and a devastating extinction event. Ice-sheet volumes claimed to be twice those of the Last Glacial Maximum paradoxically coincided with oceans as warm as today. Here we argue that some of these remarkable claims arise from undersampling of incomplete geological sections that led to apparent temporal correlations within the relatively coarse resolution capability of Palaeozoic biochronostratigraphy. We examine exceptionally complete sedimentary records from two, low and high, palaeolatitude settings. Their correlation framework reveals a Cenozoic-style scenario including three main glacial cycles and higher-order phenomena. This necessitates revision of mechanisms for the end-Ordovician events, as the first extinction is tied to an early phase of melting, not to initial cooling, and the largest $\delta^{13}C$ excursion occurs during final deglaciation, not at the glacial apex.

[1] Institut de Physique du Globe de Strasbourg, UMR7516 CNRS/Université de Strasbourg, 1 rue Blessig, 67084 Strasbourg, France. [2] Department of Earth Sciences, University of Ottawa, Ottawa, Ontario, Canada K1N 6N5. [3] Géosystèmes, UMR8217 CNRS/Université Lille 1, Avenue Paul Langevin, bâtiment SN5, 59655 Villeneuve d'Ascq, France. [4] Institut National de la Recherche Scientifique, Centre Eau Terre Environnement, 490 rue de la Couronne, Quebec City, Quebec, Canada G1K 9A9. [5] Natural Resources Canada, Geological Survey of Canada, 490 rue de la Couronne, Quebec City, Quebec, Canada G1K 9A9. [6] Université de Rennes 1, Géosciences CNRS UMR 6118, Campus de Beaulieu, 35042 Rennes, France. [7] Dipartimento di Scienze chimiche e geologiche, Università degli Studi di Cagliari, Scienze della Terra, Via Trentino, 51, 09127 Cagliari, Italy. Correspondence and requests for materials should be addressed to J.-F.G. (email: ghienne@unistra.fr).

Shelf sedimentary architecture is controlled essentially by relative rates of base-level change and sediment supply[1,2]. The base level reflects the interplay between tectonics (subsidence, volume change at mid-oceanic ridges) and the orbitally tuned, glacio-eustatically driven, sea-level change. The rate of the latter, at tens of metres per 10^4–10^5 years, is one to three orders of magnitude greater than the tectonically driven sea-level change, at tens of metres per million years or less. The critical issue for analysing the stratigraphic record, therefore, is the correct assignment of depositional units to their appropriate temporal hierarchy alongside a given sea-level curve. Another consideration is the temporal significance of the observed or suspected hiatuses. Any stratigraphic record of ancient shelf deposits, and their isotopic or palaeontological proxies, inevitably samples only the discontinuous segments of a given sea-level curve[3], which often are below the relatively coarse resolution correlation potential of Palaeozoic biostratigraphy[4]. Regardless, shelf deposits are the principal record that we have for pre-Mesozoic glaciations and they must therefore serve as stratigraphic archives for glacially driven events, providing: subsidence was active; water depths at the onset of glaciation were moderately deep; and sediment supply was adjusted to subsidence rates. These preconditions are essential for the maintenance of significant water depths during glaciation, as any rapid shallowing would pre-empt the registration of subsequent glacio-eustatic events.

The end-Ordovician witnessed one of the three largest Phanerozoic glaciations with the development of continental-scale ice sheets[5–7]. This climatic event was postulated to have been initiated by massive weathering of fresh volcanic rocks[8], tectonics and related plate motions[9–11], high cosmic ray flux impacting cloud albedo[12] or by a combination of the above[13]. The glaciation apparently coincided with highly[14] or moderately[10,15] elevated CO_2 levels, with large isotopic excursions (C, S, O, N, Nd), and with a major double-phased biological extinction[16–22]. Interpretations based on far-field, low palaeolatitude sequences, resulted in 'coup-de-théâtre' scenarios that have tied the two phases of extinction to the onset and termination of a single glaciation[16,17,21]. Yet the high palaeolatitude near-field sequences contain up to five glacial cycles that can be tentatively correlated across the Gondwanan glaciated platforms[5,23]. The low palaeolatitude archives must therefore represent a more complex scenario[18,22,24–26] than that of a single, major glacial event. If so, a multiorder climate signal with a hierarchy of cycles, a Cenozoic-type 'business as usual' scenario, is a more likely alternative than a large singular event. Such linkage of eustatic, biological and isotopic records to the climatically forced development of an ice sheet can only be contemplated within a framework of high-resolution sequence stratigraphy that integrates allo-, chemo- or biostratigraphic markers.

Here, we present such a framework, based on the recognition of genetic stratigraphic sequences (GSSs) and intervening erosion surfaces (see Methods). This framework, driven by glacio-eustatic cycles tied to the evolution of polar continental-scale ice sheets over west Gondwana[5], enables the correlation of eustatic cycles at a level that is beyond the resolution capability of most absolute dating methods and of biozones, the latter typically of Myr duration[4]. A Cenozoic-style scenario including three main glacial cycles and higher-order phenomena necessitates the revision of the end-Ordovician, glaciation-related sequence of events.

Results

Palaeolatitude sequence stratigraphic frameworks. We introduce sequence stratigraphic correlation frameworks for two superbly exposed and exceptionally well-developed latest Ordovician successions (Fig. 1), the Anti-Atlas of Morocco[7,27,28] and Anticosti Island in Canada[25,29]. Both offer sections, on a 100-km scale, from the basin edge to the axis of active sedimentary depocentres (Fig. 2 and Supplementary Figs 1 and 2). Relative to the end-Ordovician ice-sheet centre (present-day north-central Africa), they provide a near-field (Anti-Atlas, siliciclastic platform) and a far-field (Anticosti Island, mixed carbonate and siliciclastic) stratigraphic record. These two successions, up to 300 and 100 m thick, respectively, were deposited in basins with notable subsidence rates and significant (*ca.* 100 m) initial Katian water depths, enabling the development of comprehensive archives of the latest Ordovician glaciation (Supplementary Fig. 3). On the basis of average shelf-depositional rates within the overall Late Ordovician context[7,27], and on comparison with analogous late Cenozoic shelf stratigraphies[3,30], such thick successions are considered to be long-term $\gg$100 s kyr archives. In both areas, the end-Ordovician comprises three genetic low-order stratigraphic sequences (GSSs) of highest significance that, in turn, encompass a number of higher-order GSSs of intermediate and low significance (Fig. 2; see the Methods).

The intercontinental correlation of these two successions is made possible due to the recognition of marker intervals. Earlier palaeontological studies already bracketed the stratigraphic interval that contains the well-known end-Ordovician extinction events (Supplementary Figs 1 and 2). In both sections, the first extinction event is situated around the conventional Katian–Hirnantian boundary, which in our record is penecontemporaneous with the major bounding surface that separates the two lower low-order GSSs. The related 'maximum flooding interval'—rather than the maximum flooding surfaces (MFS) that cannot be strictly synchronous at the global scale—is our first marker. It correlates with the brief 'pre-Hirnantian deepening' event identified in western Laurentia[22]. The second marker based on allostratigraphy relies on the signature of the end-Ordovician glacial climax. In the Anti-Atlas, it demonstrably correlates with the stratigraphic interval bounded by glacial erosion surfaces and includes widespread glacial (subglacial, glaciomarine…) deposits in the basinal succession (the glacial interval in Fig. 2). Note that coeval strata are often absent in basin edge successions (Hajguig Wadi log in Fig. 2). In the Anticosti Island succession, the signature of the glacial climax (lowest sea levels) is ascribed to the prominent erosional unconformity at the base of the Laframboise Mb. The result is a severe erosional truncation of the studied interval (Fig. 2 and Supplementary Fig. 2). Regional correlation of low- and high-order GSSs between these two markers is indeed intriguing (Fig. 2). Moreover, other subordinate erosional unconformities at the basin edge of the Anti-Atlas succession have their counterparts in the Anticosti Island succession. For the highest-order GSSs, at least partially related to local processes, such correlations are less reliable.

The end-Ordovician glacial tempos. Within the context of glaciation, where eustasy is expected to control shallow shelf sequences[3], our findings strongly suggest that the two independent regional scale frameworks and their correlation are robust and that the correspondence of the low- and high-order GSS records from dissimilar tectonic and environmental settings arises from glacio-eustatically fluctuating sea levels, the latter a consequence of waxing and waning of the western Gondwana ice sheet. We interpret the three low-order GSSs to be the signature of the three extensive glacial cycles (Latest Ordovician Glacial Cycles, LOGCs 1–3; Figs 2 and 3 and Supplementary Note). Note that our provisional numbering refers to the latest Ordovician, understood to informally include the highest Katian and the

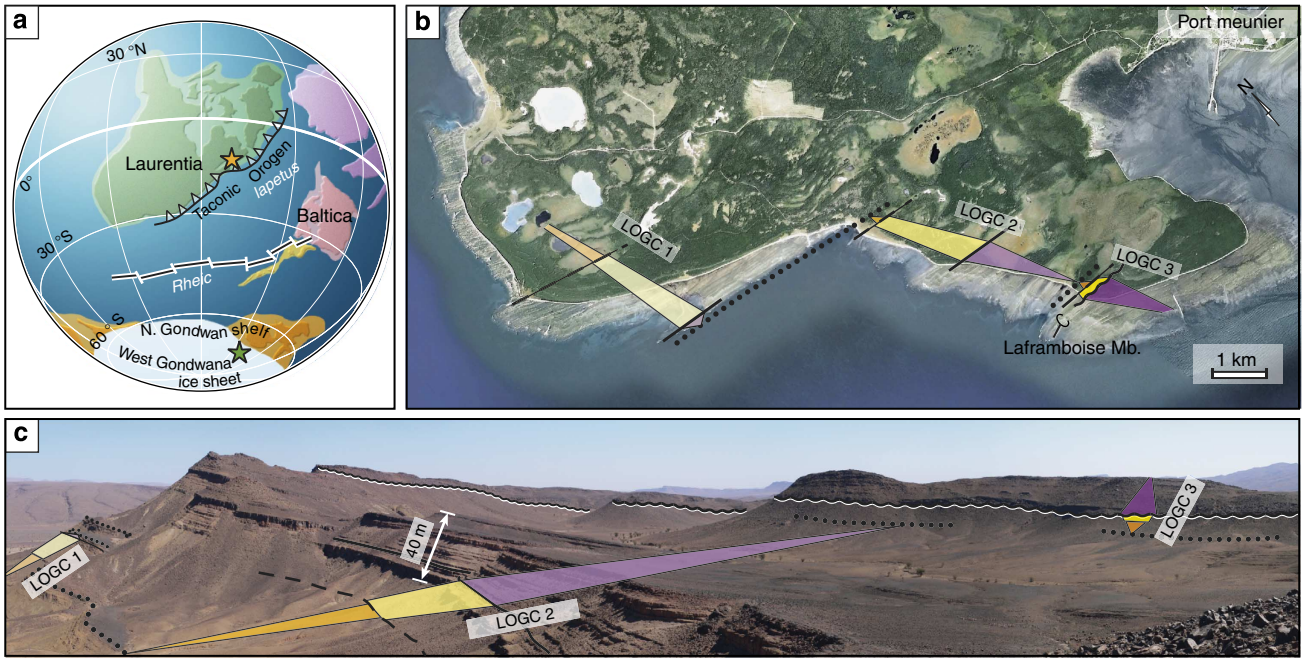

Figure 1 | Geological settings. (**a**) Position of the two study areas on a palaeogeographic reconstruction (modified from Achab and Paris[56]). In the Late Ordovician, the Anti-Atlas succession was part of the North Gondwana shelf, an epicratonic domain at high palaeolatitudes (green star). It included an actively subsiding depositional trough, which was free of ice until the middle Hirnantian, but glaciated during the glacial maximum in the upper Hirnantian. In contrast, the Anticosti Island succession accumulated in a foreland basin that developed at low palaeolatitudes during closure of the Iapetus Ocean at the onset of the Taconic orogeny (orange star). (**b**) On Anticosti Island, cliffs and marine platforms provide a superbly exposed latest Ordovician to early Silurian mixed siliciclastic–carbonate shelf succession. At Pointe Laframboise, alternating limestone (inner ramp) and softer shale (outer ramp) intervals across the shoreline platform clearly reflect the sequence stratigraphic correlation scheme inferred from sedimentary facies analysis. (**c**) Extensive outcrops of the Anti-Atlas Palaeozoic succession offer a superb record of predominantly shallow-marine Cambrian to Carboniferous sequences[27,65]. Near Tazzarine, a thick (up to 350 m) succession of alternating sandstones (storm- to tide-dominated, subordinate glaciation-related deposits) and offshore shales allows a compelling sequence stratigraphic correlation framework to be established for the latest Katian and Hirnantian (see Fig. 2). Coloured triangles represent the three identified Late Ordovician Glacial Cycles (LOGC1–3) that comprise a lower, orange/yellow triangle (regressive system tracts, RSTs) and an upper, purple triangle (transgressive system tracts, TSTs). LOGC are bounded by dotted lines, underlining MFS. Other surfaces: dashed lines, sharp-based surfaces and their correlatives within RSTs; solid lines, maximum regressive surfaces; wavy lines, subaerial erosion (Anticosti) or basal glacial erosion surface (Anti-Atlas).

Hirnantian. This is in agreement with the views that ice sheets were extant already before the latest Katian[7,22,31,32]. Our first glacial cycle spans the upper Katian (LOGC 1), the second (LOGC 2) includes the uppermost Katian strata and most of the lower to middle part of Hirnantian and the third (LOGC 3) commences in the upper Hirnantian and ends in the lowermost Silurian. In our view, corroborated recently by Nd isotope studies[22], the end-Ordovician glaciation could not have been restricted to a single short-lived glacial event, as earlier believed.

The minimum depositional time for the entire LOGC 1–3 succession is in excess of the Hirnantian duration ($\sim 1.4 \pm 0.2$ Myr[33]), the latter encompassing about 60–90% of the LOGC 2 and some 40–80% of the LOGC 3. Assuming that all LOGCs are of about equal durations, a single LOGC corresponds to a 0.7–1.6 Myr time span. The embedded higher-frequency multiorder event stratigraphy is typical of orbitally controlled climatic oscillations that lead to recurring ice-sheet growth stages[34], in agreement with the modelling results of Hermann *et al.*[35] Note however that in contrast to the well-known, strongly asymmetric and shorter-term, Pleistocene glacial cycles[36], our LOGCs show no abrupt deglaciations. They have a symmetric distribution of the high-order GSSs, as evident from the stacking patterns within the low-order regressive to transgressive system tracts (TSTs). Long-lasting interglacials are expressed as condensed, maximum flooding stratigraphic intervals[7] that account for significant portions of the overall duration of the studied time span (Fig. 3). Despite of some similarities to Quaternary glaciations[5,7,15,31,37], the durations and internal organization of LOGCs argue for dissimilar glacial tempos and forcings. These Ordovician features and tempos more closely resemble the Oligocene climate patterns that were driven by a high-amplitude obliquity modulation at 1.2 Myr frequency[34], resulting in a limited number of short-lived ice-sheet growth phases, our high-order GSSs, centred around the obliquity nodes[38,39]. Such high-frequency signals may hold some similarities to the metre-scale cycles described from other low-latitude areas and attributed to $\approx$200 (ref. 40) or 40–130 kyr (ref. 32) frequency oscillations.

Assuming the analogy with the Oligocene climate is valid, we hypothesize that an orbital forcing responding to the amplitude modulation of the obliquity typifies glacial climate systems at relatively high CO_{2atm} levels. In such a scenario, the ice-sheet inception, driven by ice-albedo feedbacks, may have resulted from a dearth of exceptionally warm rather than a ubiquity of exceptionally cool summers[38].

Discussion

Our sequence stratigraphic framework allows Hirnantian excursion(s) and extinction(s) to be revisited. The large positive carbon isotope excursions of the Palaeozoic, such as the Hirnantian Isotopic Carbon Excursion, HICE in LOGC 3 (refs 17,18,41–43), are often used as chronostratigraphic markers, albeit with no consensus model for their existence. Yet, the notion that the

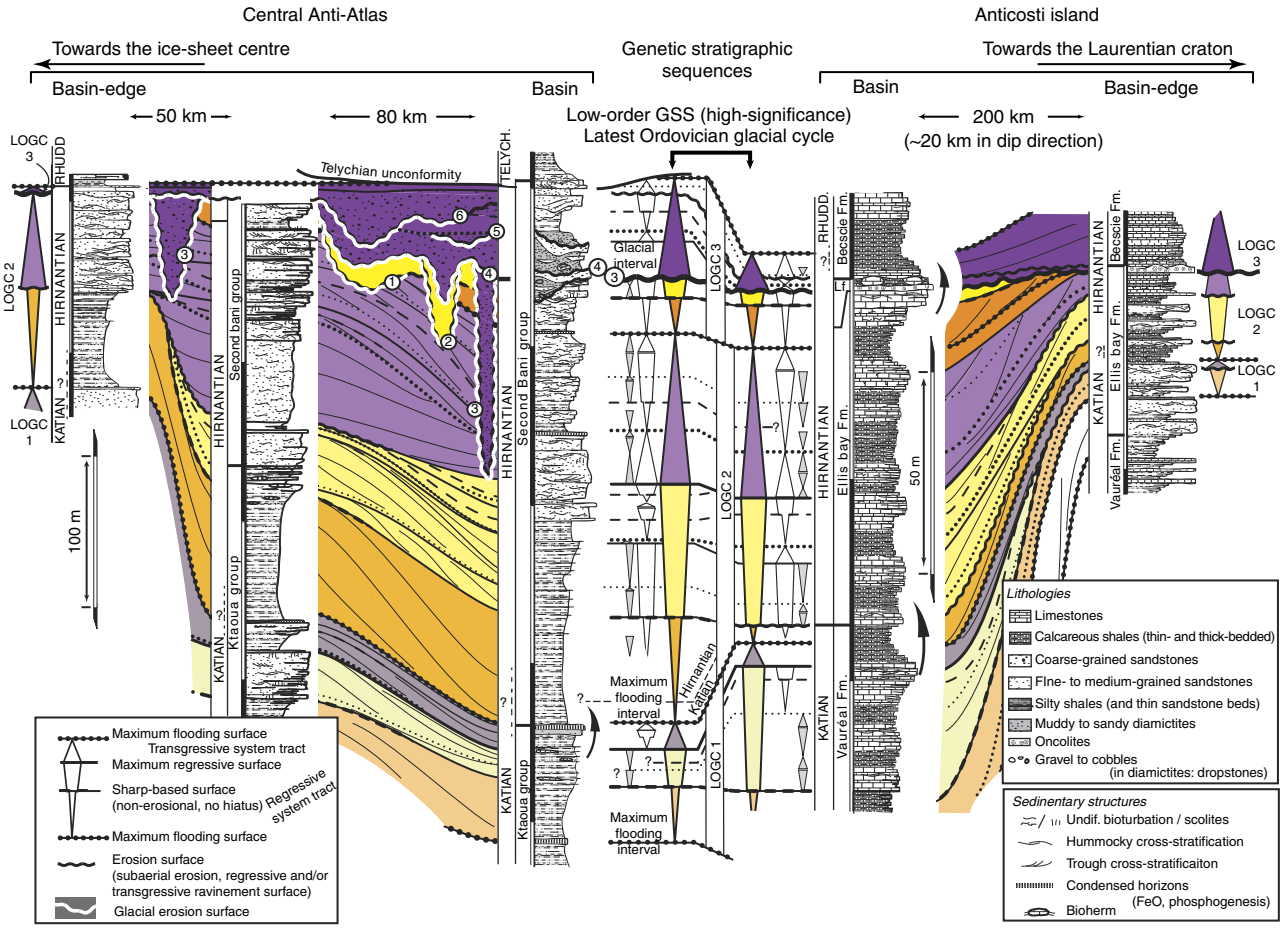

Figure 2 | Sequence stratigraphic correlation frameworks in the Anti-Atlas and Anticosti Island successions. The two frameworks were established separately and later correlated (note the different vertical scales: 50 m and 100 unit bars for the Anti-Atlas and Anticosti Island successions, respectively). Both show three superposed low-order GSSs that comprise alternating RST and TSTs symbolized by coloured, orange/yellow and purple triangles, respectively. These low-order GSSs include higher-order GSSs (high- and highest-order GSSs) of intermediate and low significance, symbolized by smaller triangles (white and grey triangles, respectively). Apparent intercontinental correlation of the two sequence stratigraphic frameworks for low- and high-order ranks confidently supports the proposition that the low-order GSSs are signatures of three successive LOGCs, which together encompass a 2–4 Myr latest Katian to lowermost Silurian time interval. Because the high- and highest-order GSSs relate to the relative rates of base-level changes (Supplementary Fig. 3), rather than to a priori assumptions about sequence duration, no temporal significance can be attributed at this stage. We retain here lithostratigraphic names because the related boundaries crosscut timelines, for example, the Katian/Hirnantian boundary (see Supplementary Figs 1 and 2). Lf: Laframboise Member. Black arrows point to stratigraphic interval with significant faunal turnovers. Encircled numbers 1–6 refer to the numbering of glacial erosion surfaces (see Supplementary Fig. 1).

$\delta^{13}C_{carb}$ signal of shelf carbonates is a direct reflection of the $\delta^{13}C_{DIC}$ of the globally uniform open ocean is clearly open to debate[13,26] (Supplementary Discussion). Note that the magnitude and occurrences of such ^{13}C enrichments depends on localized settings (for example, epeiric versus open ocean aquafacies[22,44]) and is therefore related to depositional facies and not straightforwardly to a global signal. For example, the $\delta^{13}C_{carb}$ on the modern Bahamas Bank is considerably more positive than that of the open ocean[45].

In addition, our revised chronology questions the paradigm of temporal relationships that link the position of the end-Ordovician glacial cycles, their tempos and biochemical events[13,16–22,26]. The first issue that arises is the identification and temporal range of the HICE itself. If it is understood as coeval with the large +4‰ isotopic excursion, it has to be confined to a restricted time interval of a single high-order GSS within the end-Ordovician glaciation (Fig. 3), as posited by the Anticosti case study. If, on the other hand, understood as a ^{13}C signal that commences in the latest Katian and ends in the latest Hirnantian, our results (Fig. 3 and Supplementary Table 1) show ^{13}C enrichments in at least three stratigraphic positions, suggesting that HICE combines several excursions, thus challenging its validity as a high-resolution chronostratigraphic marker.

The Anticosti $\delta^{13}C_{carb}$ curve (Fig. 3) includes two main isotopic events. First, it is the well-known excursion in the Laframboise Mb. (+4‰) that is disconnected from a rising limb in the underlying strata by a major unconformity that we relate to the glacial maximum and to subaerial erosion in LOGC 3. Second, there is an earlier asymmetric excursion (+2‰) with its descending limb that is spanning the lower and middle parts of the Ellis Bay Fm. (LOG 2). There is also a lesser enrichment in the uppermost Vauréal Fm., associated with LOGC 1, which may form a third, subordinate excursion. Other putative (<1‰) excursions, while present, are minor and difficult to interpret. This multi-peak isotope pattern at Anticosti Island questions the views of strictly synchronous signals, despite observations that a number of Hirnantian records worldwide—and potentially similar 'wiggles' in the carbon isotope record elsewhere—contain positive $\delta^{13}C$ spikes that appear isochronous[17,24,46] within the correlation capabilities of the Palaeozoic bio- and/or

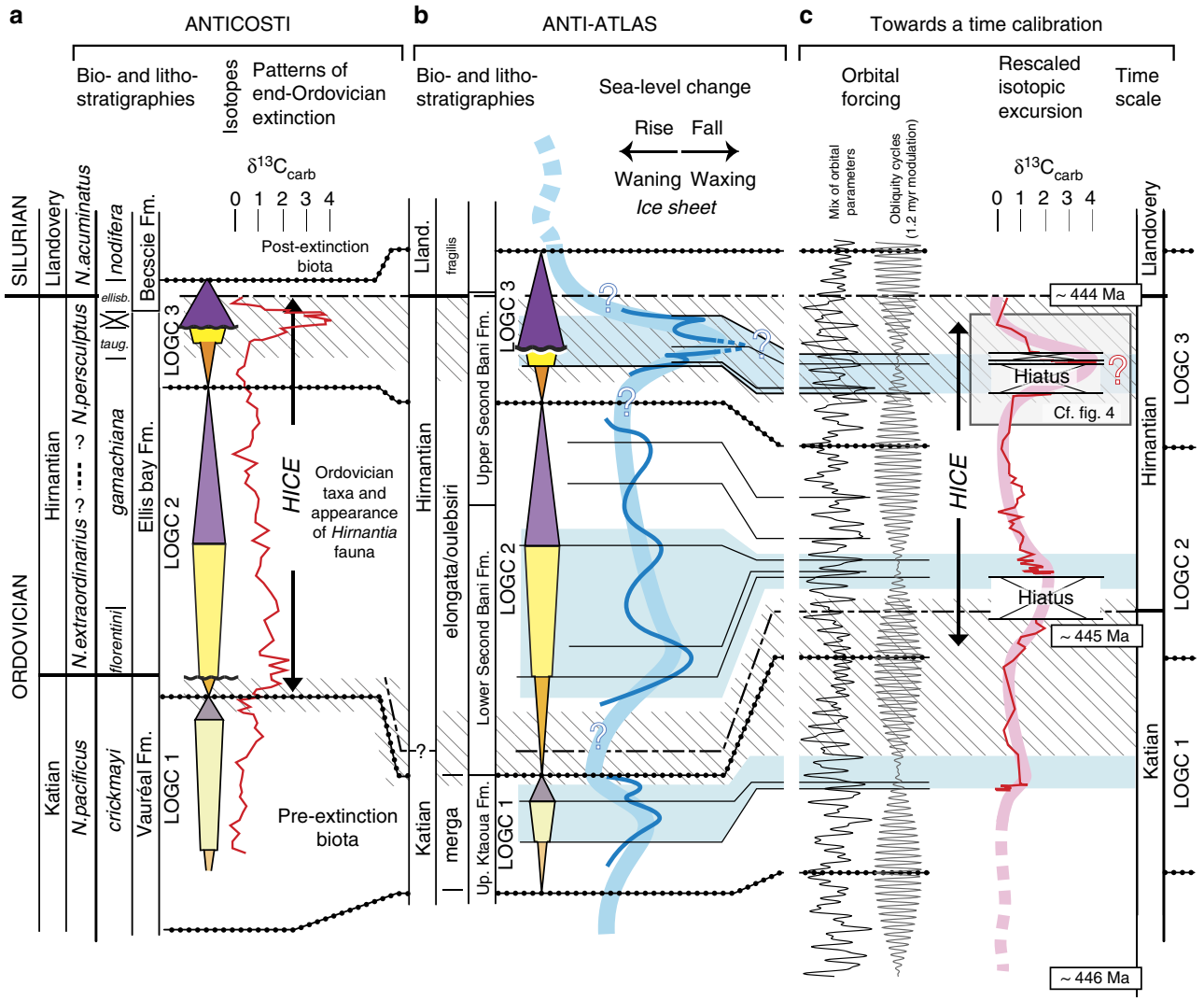

Figure 3 | Perspective of sequence stratigraphy. Temporal correspondence between documented (chitinozoa[54,55,59,60]) or essentially inferred (graptolite) biostratigraphies and (**a**), the Anticosti Island succession with its related isotopic signal and faunal turnovers and (**b**), the Anti-Atlas succession with interpreted low-frequency sea-level changes and ice-sheet occurrences. A cycle hierarchy is developed that distinguishes LOGC1–3 (low-order, high-significance Late Ordovician Glacial Cycles represented by both coloured triangles and the thick, pale blue curve) from high-order cycles (thin, dark blue curve). LOGCs are bounded by major MFS (dotted lines). Blue shading highlights time intervals specifically characterized, or thought to be characterized by ice-sheet development stages. The ice-sheet development increased from the late Katian to the late Hirnantian, as suggested by glacioeustatic trends. The dashed blue curve is a representation of the early Silurian eustatic background. Black, dashed lines are the inferred Katian to Hirnantian and Hirnantian to Llandovery boundaries. (**c**) Representation of a potential time calibration is based on astronomical forcings dominated by 1.2 Myr amplitude modulation of obliquity cycles[34] (see text for details). By analogy with the Cenozoic, the composite artificial curve was constructed by mixing high-frequency orbital cycles ('ETP' for eccentricity–tilt–climatic precession[33]) and here it is shown only to illustrate the distortion in the stratigraphic record. It results in condensed transgressive and overdeveloped lowstand intervals, relative to a linear timescale. The high- and highest-order glacial cycles likely correspond to such orbitally forced, high-frequency climatic oscillations. In contrast, during the long interglacials orbital forcing did not result in ice-sheet development and they have therefore a poorly differentiated record. The end-Ordovician includes short glaciation intervals with cumulative duration of perhaps a few hundred thousand years. The embedded isotopic and biological signals show up to three discrete isotopic events and two faunal turnovers (oblique-line shading), from the highest Katian to uppermost Hirnantian. The Hirnantian isotopic carbon excursion (HICE) is not restricted to the excursion associated with LOGC 3 at the top of the Ellis Bay Fm. The dashed pink curve is a representation of the Katian isotopic background.

chronostratigraphy[26]. An apparent single peak may represent only disjointed parts (Fig. 4) of a hypothetically complete $\delta^{13}C_{carb}$ curve for just one of several repetitious LOGCs, or a composite signal from an artificially stacked section.

Whatever the temporal extent of HICE, our sequence stratigraphic framework warrants reconsideration of the published 'cause-and-effect' scenarios for its origin. The rising limb of the ^{13}C excursion at the base of the Ellis Bay Fm. (Fig. 3) is associated with a highstand that follows the LOGC 1–2 transition, while its descending limb spans several high-frequency glacio-eustatic cycles within the late regressive to TSTs of the LOGC 2. In this case, there is therefore no apparent connection between eustasy and the $\delta^{13}C_{carb}$ curve. The simplest explanation is to see the LOGC 2 isotopic signal as that of regional epeiric water masses with their distinctive variations in $\delta^{13}C$ (ref. 44). In contrast, the subsequent, exceptionally high-amplitude excursion is within the TST of LOGC 3, and is associated with a drastic basin-scale change of facies caused by transition from glacial to

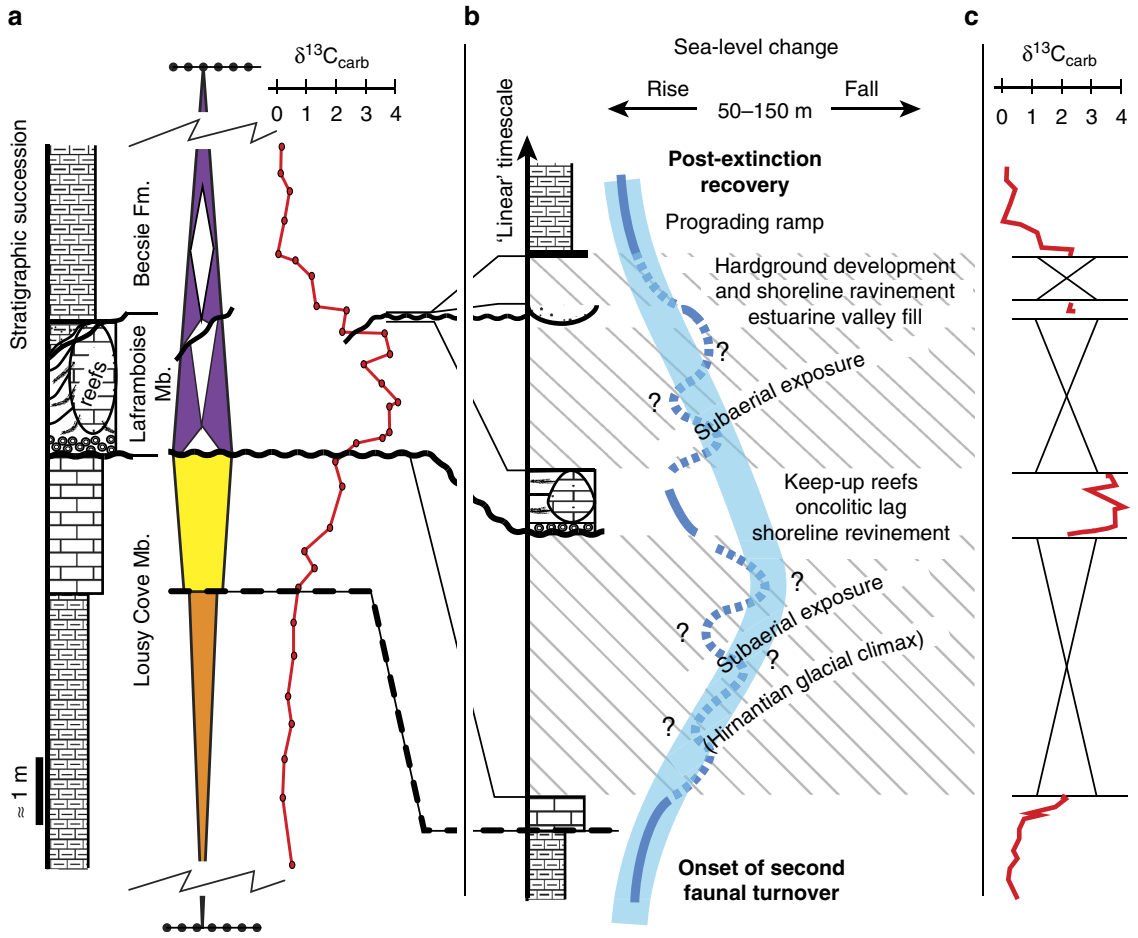

Figure 4 | A detailed interpretation of the far-field LOGC 3 stratigraphic and isotopic record. (**a**) The main lithostratigraphic units on Anticosti Island, including the Laframboise Member, are shown with their representative depositional facies and related $\delta^{13}C$ curve. They are separated by shoreline ravinement unconformities[62]. The sequence stratigraphic interpretation differentiates low-order/high-significance regressive (orange and yellow triangle) and transgressive (purple triangle) system tracts. The corresponding first-order unconformity coincides with the base of the Laframboise Member. High-order cycles represented by white triangles are present in the LOGC 3 TST, which commences with the base of the Laframboise Member. (**b**) The same sequence in the 'linear' timescale perspective of this succession of depositional events. It includes relatively long depositional hiatuses (oblique-line shading). At Anticosti, the high-frequency glacio-eustatic sea level changes, similar to those recorded in the near-field glacial record of Morocco, are represented by unconformities coeval with the glacial maxima. One recorded interglacial event (Laframboise Mb.) is interpreted here as a single high-order GSS within the larger TST of LOGC 3. (**c**) An alternative view of the isotopic excursion, which includes the stratigraphic hiatuses. The $\delta^{13}C$ record captures only disjointed segments of the isotope signal. In particular, the $\delta^{13}C$ curve does not include values from the time interval that corresponds to the Hirnantian glacial climax. We suspect that the trend from background levels to the maximum in fact combines an initial rise that predates the glacial climax, the associated hiatus and the subsequent maximum that postdates the glacial climax. This maximum is developed mainly within the reefal limestones constituting the highstand facies of a particular high-order GSS.

warmer climates (reefs of the Laframboise Mb.). At a higher resolution, the excursion appears to be confined to the highstand of a high-order GSS (Fig. 4), thus peaking at times of rising sea levels associated with deglaciation. This coincidence is opposite to the postulated lowstand conditions that are essential in the 'weathering' scenario[11] and the model can be discounted as a potential explanation. The 'productivity'[47] and related 'circulation pattern' explanations[48,49] could perhaps offer plausible alternatives, providing it can be demonstrated that the isotopic excursion is not facies dependent. Our highstand nadir of isotope excursion can then be consistent with the scenario that invokes carbon storage in the deeper parts of the shelf[39], albeit constrained—because of it high amplitude—to basinal, not global, scales (see box model in Supplementary Discussion and Supplementary Tables 2 and 3). In such a context, the particular highstand conditions favourable for the development of carbon excursions may arise at distinct locations during any high-order GSSs. If so, it is the short duration of contiguous high-order GSSs that give the impression of a synchronous, worldwide phenomenon during the LOGC 3 transgressive trends. For minor excursions, such as those in LOGC 1 or in the uppermost (below the unconformity) Ellis Bay Fm., we contend that our present-day knowledge of carbon isotope systematics does not permit unique diagnostics of causative factors and scenarios. We therefore desist from their interpretation.

In summary, providing our sections represent sufficiently comprehensive archives of the latest Ordovician development, we dispute the apparent association of each LOGC with an individual isotopic excursion. At higher resolution, the relationship with sea-level history differs from case to case, indicating that it is not a unique forcing but likely a combination of processes that is involved in ^{13}C enrichment[21].

Similar reasoning may suggest that 'pulses' in patterns of the end-Ordovician biological extinction result from telescoping of

segments from the stratigraphic record, as must be the case for hiatus-dominated successions[20]. The two phases of the Late Ordovician mass extinction that were documented worldwide in earlier studies[17,21] are however confirmed also by our results on the Anticosti Island (Fig. 3 and Supplementary Fig. 2). Our correlation framework moreover indicates that these turnovers are relatively long-lasting time intervals that encompass several glacio-eustatic fluctuations of the high or highest GSSs in the Anti-Atlas record. Whether these turnovers originate from evolution specifically related to LOGC developments, or whether they only mirror a succession of stacked, quasi-instantaneous, pulses is beyond resolution of our data set, regardless of their potential combination within protracted, global events[21,50]. The ensemble of our sections studied represents only a fraction of affected palaeohabitats and biota, and, as explained, sections that contain complementary palaeontological data cannot be readily correlated into our framework; our analyses thus likely undersamples the full biotic dynamics through this interval. Yet, our juxtaposition of extinction phases to glacial development suggests a more nuanced scenario than previously advocated (Fig. 3).

The older turnover, which has classically been associated with the onset of the Hirnantian glaciation at the base of the *N. extraordinarius* Biozone, spans an interval that includes LOGC 1 deglaciation and the early LOGC 2 highstand. This turnover corresponds therefore mostly to the first major interglacial period. The models that are based on processes linked to glacial onset, such as the shrinkage of biotic ecospace, temperature decline or development (or the loss) of anoxia during falling sea level[13,15,20,21], are thus not compatible with this revised scenario. Instead, processes linked to deglaciation dynamics (for example, amplification of meltwater fluxes that enhance ocean stratification), or flooding of the shelves by relatively deep anoxic waters[13,21,51], appear to be more likely scenarios for this first turnover, but they are not applicable, as previously envisioned, for the second turnover. The second turnover that we recognize in LOGC 3 is an event traditionally assigned to the lower part of the *N. persculptus* Biozone. This extinction/recovery pattern affects mostly macrofauna in the Anticosti Island succession (Supplementary Fig. 2). The phytoplankton crisis, on the other hand, commenced beneath the regional unconformity (Fig. 4), that is before glacial climax of LOGC 3 (refs 42,52), suggesting that the second end-Ordovician faunal turnover may have been initiated already during the late Hirnantian ice-sheet waxing, thus casting doubt on a unique causative linkage that would have been confined to final deglaciation. Note nevertheless that the ubiquitous existence of worldwide hiatuses at that time makes any interpretation tentative.

While we appreciate the merits of a sophisticated model-driven approach, and welcome the impetus derived from it, the insights arising here from the application of basic geological methods underline the need for detailed understanding of the rock record as well[13]. In this contribution, temporal relationships of near-field and far-field records for the end-Ordovician glaciation are considered within a high-resolution, multiorder correlation framework that reflects a Cenozoic-style hierarchy of glacio-eustatically driven oscillations consisting of three main cycles and superimposed higher-order subcycles. This interpretation questions earlier views that were based on lower resolution data sets for a simple latest Katian decline in sea level followed by its rise in the upper Hirnantian. An oversimplified sedimentary succession likely incorporates significant hiatuses and represents only a partial record of the entire time interval[18,53]. Frequently, such stratigraphic sections correspond to vertically juxtaposed, unrelated parts of glacial cycles, resulting in biased timing of biochemical signals relative to the glacial tempos. On the basis of our framework, we anticipate that the most easily captured phases in the worldwide end-Ordovician development should reflect the initial waxing stage and potentially the immediately ensuing flooding event (LOGC 1), followed by later reflooding of the shelves at the end of LOGC 3. In more comprehensive successions, the maximum flooding interval at the LOGC 2-3 transition (mid-Hirnantian transgression[5]) will likely yield a decipherable signature[22].

The orbitally controlled depositional record of a glacial interval will mostly be underrepresented in proven or suspected hiatuses. These may originate from nondeposition, subaerial or subglacial unconformities, transgressive post-glacial ravinement processes, mass movements or from erosion by bottom currents, the latter being particularly effective for the deeper parts of shelf basins. Due to the lack of Palaeozoic deep-sea records, the absolute timing and calibration of the Ordovician glaciation may remain enigmatic[13]. We envision therefore that future progress in understanding the temporal, spatial and causal evolution of the Late Ordovician environmental record will have to rely on high-resolution methods that capture multiorder sequence stratigraphy and related proxies along depositional profiles on a regional scale. Our advances using these methods include: rejection of the earlier cause-and-effect scenarios for HICE(s), as these no longer fit with the revised context of glacial/ glacio-eustatic development; the suggestion that low-order LOGCs likely represent the 1.2 Myr long obliquity cycles that modulated ice-sheet dynamics, similar to scenarios proposed for the Oligocene; and the insight that the first Hirnantian extinction pulse, contrary to earlier studies, was linked to an intervening melting phase, not to the initial cooling phase of the end-Ordovician.

Methods

GSSs. Sequence stratigraphic correlation frameworks are based on visual correlations of marker beds along continuous exposures at the 10–30 km scale (Fig. 2) and on refined, regional scale, chitinozoan-based biostratigraphies for northern Gondwana[54–58] and eastern Laurentia[59,60]. This results in correlations that are noticeably different from lithostratigraphic schemes (Supplementary Figs 1 and 2). MFS and a variety of erosion surfaces have been delineated in the field. The MFS coincide with deeper, usually condensed, depositional conditions and serve as bounding surfaces for GSSs[61], ideally including a lower regressive system tract (RST) and an upper transgressive system tract (TST). Erosional surfaces correspond to glacial erosion surfaces (Morocco); subaerial unconformities reworked by transgressive ravinement processes (SR-U sensu Embry, 2009 (ref. 62); Anticosti); or sharp-based erosional surfaces punctuating regressive facies trends and ascribed in most cases to regressive surfaces of marine erosion (Anti-Atlas and Anticosti). We favour GSSs over Trangressive/Regressive[62] (T–R), or depositional sequences[2] because their bounding surfaces (MFS) better approximate late deglaciation conditions and thus appropriately bracket glacial cycles. In this scheme, a post-glacial highstand of an interglacial is represented by deposits that constitute the lower part of the subjacent sequence.

Sequence hierarchy. Stratigraphic surfaces have been assigned to a hierarchy of GSSs. The significance of facies shifts and/or their penetration into the basin are used as criteria to assess the relative magnitude of base-level falls in successive, multiorder sequences. It results in a data-driven hierarchy[62], different from a frequency-related scheme based on a priori assumptions about durations of sequences. The highest-order (low significance) GSSs display limited facies shifts, both in the basin and at basin edge. More significant are the high-order genetic sequences, which comprise several highest-order GSSs and/or include abrupt facies shifts associated with coeval, or at least suspected, erosion surfaces at basin edge. The low-order sequences (highest significance) are made up of a suite of high-order sequences, the stacking pattern of which defines long-term RST and TST. They are bounded by the major MFS associated with severe condensation (for example, phosphogenesis in the Anti-Atlas). They include in their most regressive part (late RST or early TST) one or several important erosional surfaces such as shoreline ravinement unconformities, or glacial erosion surfaces in the upper Hirnantian in Morocco, which expand toward basinal areas. This approach is often not appropriate for maximum flooding intervals characterized by relatively deep depositional conditions, where facies shifts are poorly deciphered. Here, an alternative, frequency-related, hierarchy is frequently applied[7].

Base-level falls associated with glacial erosional surfaces are recognized on the basis of: their basinward extent at regional scale[63] (Supplementary Fig. 1); the development/absence of well-organized subglacial shear zones that indicate fully

subglacial/marginal ice fronts[64]. Maximum erosional depths are not considered to be a measure of the significance of a glacial surface. We are aware that such estimates reflect glacial extents rather than true ice-sheet volumes, but they do have significance when dealing with high- and low-order GSSs.

References

1. Jervey, M. T. in *Sea Level Changes—An Integrated Approach* Vol. 42 (eds Wilgus, C. K. *et al.*) 47–69 (Society of Economic Paleontologists and Mineralogists, Special Publication, 1988).
2. Catuneanu, O. *et al.* Towards the standardization of sequence stratigraphy. *Earth-Sci. Rev.* **92,** 1–33 (2009).
3. Mountain, G. S. *et al.* in *Continental Margin Sedimentation: From Sediment Transport to Sequence Stratigraph* Vol. 37 (eds Nittrouer, C. A. *et al.*) 381–458 (International Association of Sedimentologists, Special Publication, Blackwells, 2007).
4. Sadler, P. M., Cooper, R. A. & Melchin, M. High-resolution, early Paleozoic (Ordovician-Silurian) time scales. *GSA Bull.* **121,** 887–906 (2009).
5. Ghienne, J.-F., Le Heron, D., Moreau, J., Denis, M. & Deynoux, M. in *Glacial Sedimentary Processes and Products* Vol. 39 (eds Hambrey, M. *et al.*) 295–319 (International Association of Sedimentologists, Special Publication, Blackwells, 2007).
6. Le Heron, D. P. & Craig, J. First-order reconstructions of a Late Ordovician Saharan ice sheet. *J. Geol. Soc.* **165,** 19–29 (2008).
7. Loi, A. *et al.* The Late Ordovician glacio-eustatic record from a high latitude storm-dominated shelf succession: the Bou Ingarf section (Anti-Atlas, Southern Morocco). *Palaeogeogr. Palaeocl. Palaeoecol.* **296,** 332–358 (2010).
8. Lefebvre, V., Servais, T., François, L. & Averbuch, O. Did a Katian large igneous province trigger the Late Ordovician glaciation? A hypothesis tested with a carbon cycle model. *Palaeogeogr. Palaeocl. Palaeoecol.* **296,** 309–319 (2010).
9. Herrmann, A. D., Patzkowsky, M. E. & Pollard, D. The impact of paleogeography, *p*CO2, poleward ocean heat transport, and sea level change on global cooling during the Late Ordovician. *Palaeogeogr. Palaeocl. Palaeoecol.* **206,** 59–74 (2004).
10. Nardin, E. *et al.* Modeling the early Paleozoic long-term climatic trend. *Geol. Soc. Am. Bull.* **123,** 1181–1192 (2011).
11. Kump, L. R. *et al.* A weathering hypothesis for glaciation at high atmospheric pCO_2 during the Late Ordovician. *Palaeogeogr. Palaeocl. Palaeoecol.* **152,** 173–187 (1999).
12. Shaviv, N. J. & Veizer, J. Celestial driver of Phanerozoic climate? *GSA Today* **13/7,** 4–10 (2003).
13. Melchin, M. J., Mitchell, C. E., Holmden, C. & Štorch, P. Environmental changes in the Late Ordovician–early Silurian: Review and new insights from black shales and nitrogen isotopes. *GSA Bull.* **125,** 1635–1670 (2013).
14. Royer, D. L. CO_2-forced climate thresholds during the Phanerozoic. *Geochim. Cosmochim. Acta* **70,** 5665–5675 (2006).
15. Vandenbroucke, T. R. A. *et al.* Polar front shift and atmospheric CO_2 during the glacial maximum of the Early Paleozoic Ice-house. *Proc. Natl Acad. Sci. USA* **107,** 14983–14986 (2010).
16. Sheehan, P. M. The Late Ordovician mass extinction. *Annu. Rev. Earth Planet. Sci.* **29,** 331–364 (2001).
17. Brenchley, P. J. *et al.* High-resolution stable isotope stratigraphy of Upper Ordovician sequences: Constraints on the timing of bioevents and environmental changes associated with mass extinction and glaciation. *Geol. Soc. Am. Bull.* **115,** 89–104 (2003).
18. Bergström, S. M., Saltzman, M. R. & Schmitz, B. First record of the Hirnantian (Upper Ordovician) $\delta^{13}C$ excursion in the North American Midcontinent and its regional implications. *Geol. Mag.* **143,** 657–678 (2006).
19. Finnegan, S. *et al.* The magnitude and duration of Late Ordovician-Early Silurian glaciation. *Science* **331,** 903–906 (2011).
20. Finnegan, S., Heim, N. A., Peters, S. E. & Fisher, W. W. Climate change and the selective signature of the Late Ordovician mass extinction. *Proc. Natl Acad. Sci. USA* **109,** 6829–6834 (2012).
21. Harper, D. A. T., Hammarlund, E. U. & Rasmussen, C. M. Ø. End Ordovician extinctions: a coincidence of causes. *Gondwana Res.* **25,** 1294–1307 (2013).
22. Holmden, C. *et al.* Nd isotope records of late Ordovician sea-level change—Implications for glaciation frequency and global stratigraphic correlation. *Palaeogeogr. Palaeocl. Palaeoecol.* **386,** 131–144 (2013).
23. Sutcliffe, O. E., Dowdeswell, J. A., Whittington, R. J., Theron, J. N. & Craig, J. Calibrating the Late Ordovician glaciation and mass extinction by the eccentricity cycles of the Earth's orbit. *Geology* **23,** 967–970 (2000).
24. Melchin, M. J. & Holmden, C. Carbon isotope chemostratigraphy in Arctic Canada: Sea-level forcing of carbonate platform weathering and implications for Hirnantian global correlation. *Palaeogeogr. Palaeocl. Palaeoecol.* **234,** 186–200 (2006).
25. Desrochers, A., Farley, C., Achab, A., Asselin, E. & Riva, J. F. A far-field record of the end Ordovician glaciation: the Ellis Bay Formation, Anticosti Island, Eastern Canada. *Palaeogeogr. Palaeocl. Palaeoecol.* **296,** 248–263 (2010).
26. Delabroye, A. & Vecoli, M. The end-Ordovician glaciation and the Hirnantian Stage: a global review and questions about Late Ordovician event stratigraphy. *Earth-Sci. Rev.* **98,** 269–282 (2010).
27. Destombes, J., Hollard, H. & Willefert, S. in *Lower Palaeozoic of North-western and West Central Africa* (ed. Holland, C. H.) 91–336 (John Wiley, 1985).
28. Le Heron, D. Late Ordovician glacial record of the Anti-Atlas, Morocco. *Sediment. Geol.* **201,** 93–110 (2007).
29. Long, D. G. F. Tempestite frequency curves: a key to Late Ordovician and Early Silurian subsidence, sea-level change, and orbital forcing in the Anticosti foreland basin, Quebec, Canada. *Can. J. Earth Sci.* **44,** 413–431 (2007).
30. Janszen, A., Spaak, M. & Moscariello, A. Effects of the substratum on the formation of glacial tunnel valleys: an example from the Middle Pleistocene of the southern North Sea Basin. *Boreas* **41,** 629–643 (2012).
31. Vandenbroucke, T. R. A. *et al.* Ground-truthing Late Ordovician climate models using the paleobiogeography of graptolites. *Palaeoceanography* **24,** PA4202 (2009).
32. Elrick, M. *et al.* Orbital-scale climate change and glacioeustasy during the early Late Ordovician (pre-Hirnantian) determined from $\delta^{18}O$ values in marine apatite. *Geology* **41,** 775–778 (2013).
33. Gradstein, F. M. *et al. The Geologic Time Scale* (Elsevier, 2012).
34. Boulila, S. *et al.* On the origin of Cenozoic and Mesozoic 'third-order' eustatic sequences. *Earth-Sci. Rev.* **109,** 94–112 (2011).
35. Hermann, A. D., Patzkowsky, M. E. & Pollard, D. Obliquity forcing with 8–12 times preindustrial levels of atmospheric pCO_2 during the Late Ordovician glaciation. *Geology* **31,** 485–488 (2003).
36. Waelbroeck, C. *et al.* Sea-level and deep water temperature changes derived from benthic foraminifera isotopic records. *Quaternary Sci. Rev.* **21,** 295–305 (2002).
37. Armstrong, H. A. in *Deep Time Perspectives on Climate Change* (eds Williams, M., Haywood, A., Gregory, F. J. & Schmidt, D. N.) 101–121 (Special Publication of the Geological Society of London, The Micropalaeontological Society and Geological Society of London, London, 2007).
38. Zachos, J. C., Shackleton, N. J., Revenaugh, J. S., Pälike, H. & Flower, B. P. Climate response to orbital forcing across the Oligocene-Miocene Boundary. *Science* **292,** 274–278 (2001).
39. Wade, B. S. & Pälike, H. Oligocene climate dynamics. *Paleoceanography* **19,** PA4019 (2004).
40. Williams, G. E. Milankovitch-band cyclicity in bedded halite deposits contemporaneous with Late Ordovician-Early Silurian glaciation, Canning Basin, Western Australia. *Earth Planet. Sci. Lett.* **103,** 143–155 (1991).
41. LaPorte, D. F. *et al.* Local and global perspectives on carbon and nitrogen cycling during the Hirnantian glaciation. *Palaeogeogr. Palaeocl. Palaeoecol.* **276,** 182–195 (2009).
42. Young, S., Saltzman, M. R., Ausich, W. I., Desrochers, A. & Kaljo, D. Did changes in atmospheric CO_2 coincide with latest Ordovician glacial-interglacial cycles? *Palaeogeogr. Palaeocl. Palaeoecol.* **296,** 376–388 (2010).
43. Munnecke, A., Calner, M., Harper, D. A. T. & Servais, T. Ordovician and Silurian sea–water chemistry, sea level, and climate: a synopsis. *Palaeogeogr. Palaeocl. Palaeoecol.* **296,** 389–413 (2010).
44. Holmden, C., Creaser, R. A., Muehlenbachs, K., Leslie, S. A. & Bergström, S. M. Isotopic evidence for geochemical decoupling between ancient epeiric seas and bordering oceans: implications for secular curves. *Geology* **26,** 567–570 (1998).
45. Swart, P. & Kennedy, M. J. Does the global stratigraphic reproducibility of $\delta^{13}C$ in Neoproterozoic carbonates require a marine origin? A plio-Pleistocene comparison. *Geology* **40,** 87–90 (2012).
46. Fan, J., Peng, P. & Melchin, M. J. Carbon isotopes and event stratigraphy near the Ordovician–Silurian boundary, Yichang, South China. *Palaeogeogr. Palaeocl. Palaeoecol.* **276,** 160–169 (2009).
47. Brenchley, P. J. *et al.* Bathymetric and isotopic evidence for a shortlived Late Ordovician glaciation in a greenhouse period. *Geology* **22,** 295–298 (1994).
48. Jeppson, L. & Calner, M. The Silurian Mulde Event and a scenario for a secundo-secundo events. *T. Roy. Soc. Edin. Earth Sci.* **93,** 135–154 (2003).
49. Cramer, B. S. & Saltzman, M. R. Fluctuations in epeiric sea carbonate production during Silurian positive carbon isotope excursions: A review of proposed paleoceanographic models. *Palaeogeogr. Palaeocl. Palaeoecol.* **245,** 37–45 (2007).
50. Rasmussen, C. M. O. & Harper, D. A. T. Did the amalgamation of continents drive the end Ordovician mass extinctions? *Palaeogeogr. Palaeocl. Palaeoecol.* **311,** 48–62.
51. Hammarlund, E. U. *et al.* A sulphidic driver for the end-Ordovician mass extinction. *Earth Planet. Sci. Lett.* **331,** 128–139 (2012).
52. Delabroye, A. *et al.* Phytoplankton dynamics across the Ordovician/Silurian boundary at low palaeolatitudes: Correlations with carbon isotopic and glacial events. *Palaeogeogr. Palaeocl. Palaeoecol.* **312,** 79–97 (2011).

53. Bergström, S. M., Lehner, O., Calner, M. & Joachimski, M. A new upper Middle Ordovician-Lower Silurian drillcore standart succession from Borenshult in Östergötland, southern Sweden: 2. Significance of $\delta^{13}C$ chemostratigraphy. *GFF* **134,** 39–63 (2012).
54. Bourahrouh, A., Paris, F. & Elaouad-Debbaj, Z. Biostratigraphy, bodiversity and palaeoenvironments of the chitinozoans and associated palynomorphs from the Upper Ordovician of the Central Anti-Atlas, Morocco. *Rev. Palaeobot. Palyno.* **130,** 17–40 (2004).
55. Webby, B. D., Cooper, R. A., Bergström, S. M. & Paris, F. in *The Great Ordovician Diversification Event* (eds Webby, B. D., Paris, F., Droser, M. & Percival, I.) 41–47 (Columbia University Press, 2004).
56. Achab, A. & Paris, F. The Ordovician chitinozoan biodiversification and its leading factors. *Palaeogeogr. Palaeocl. Palaeoecol.* **245,** 5–19 (2007).
57. Paris, F. *et al.* Palynological and palynofacies analysis of early Silurian shales from borehole CDEG-2a in Dor el Gussa, eastern Murzuq Basin, Libya. *Rev. Palaeobot. Palyno.* **174,** 1–26 (2012).
58. Paris, F. *et al.* Late Ordovician-earliest Silurian chitinozoans from the Qusaiba core hole (North Central Saudi Arabia) and relation to the Hirnantian glaciation. *Rev. Palaeobot. Palyn.* (in the press).
59. Achab, A., Asselin, E., Desrochers, A., Riva, J. F. & Farley, C. Chitinozoan biostratigraphy of a new Upper Ordovician stratigraphic framework for Anticosti Island, Canada. *Geol. Soc. Am. Bull.* **123,** 186–205 (2011).
60. Achab, A., Asselin, E., Desrochers, A. & Riva, J. F. The end-Ordovician chitinozoan zones of Anticosti Island, Québec: definition and stratigraphic position. *Rev. Palaeobot. Palyno.* **198,** 92–109 (2013).
61. Galloway, W. E. Genetic stratigraphic sequences in basin analysis. I. Architecture and genesis of flooding-surface bounded depositional units. *Amer. Assoc. Petr. Geol. Bull.* **73,** 125–142 (1989).
62. Embry, A. F. Practical sequence stratigraphy. Canadian Society of Petroleum Geologists. at www.cspg.org (2009).
63. Le Heron, D., Ghienne, J.-F., El Houicha, M., Khoukhi, Y. & Rubino, J.-L. Maximum extent of ice sheets in Morocco during the Late Ordovician glaciation. *Palaeogeogr. Palaeocl. Palaeoecol.* **245,** 200–226 (2007).
64. Denis, M., Guiraud, M., Konaté, M. & Buoncristiani, J.-F. Subglacial deformation and water-pressure cycles as a key for understanding ice stream dynamics: evidence from the Late Ordovician succession of the Djado Basin (Niger). *Int. J. Earth Sci.* **99,** 1399–1425 (2010).
65. Burkhard, M., Caritg, S., Helg, U., Robert-Charrue, C. & Soulaimani, S. Tectonics of the Anti-Atlas of Morocco. *C. R. Geosci.* **338,** 11–24 (2006).

Acknowledgements

J.-F.G. and T.R.A.V. acknowledge financial support from the French 'Agence Nationale de la Recherche' through grant ANR-12-BS06-0014 'SEQSTRAT-ICE', the CNRS (action SYSTER) and the Regional Council of Nord-Pas de Calais (emergent projects action) in France. This is a contribution to IGCP 591 'The Early to Middle Palaeozoic Revolution'. A.D., J.V. and S.W. acknowledge support from NSERC.

Author contributions

J.-F.G., M.-P.D. and A.L. and A.D., C.F., S.W. and J.V. compiled and generated field data, from the Anti-Atlas and the Anticosti Island, respectively. T.R.A.V. and F.P. and A.A. and E.A. generated biostratigraphic data for the Anti-Atlas and the Anticosti Island, respectively. S.W. and J.V. performed isotopic data and ran the C-cycle model. J.-F.G., A.D., T.R.A.V. and J.V. designed the research and wrote the paper.

Additional information

Supplementary Information accompanies this paper at http://www.nature.com/naturecommunications

Competing financial interests: The authors declare no competing financial interests.

Reprints and permission information is available online at http://npg.nature.com/reprintsandpermissions/

How to cite this article: Ghienne, J.-F. *et al.* A Cenozoic-style scenario for the end-Ordovician glaciation. *Nat. Commun.* 5:4485 doi: 10.1038/ncomms5485 (2014).

SUPPLEMENTARY INFORMATION

Supplementary Figures

Supplementary Tables

Supplementary Note: The essentials of the three Late Ordovician Glacial Cycles

Supplementary Discussion: Box model of the late Ordovician carbon cycle

Supplementary References

Supplementary Figure 1

Bio-, and lithostratigraphy in the Anti-Atlas. In southern Morocco, the end-Ordovician record (**a**-**d**) is part of the up to 5 km thick Palaeozoic succession preserved in the central Anti-Atlas depositional trough (**e**, modified from Destombes et al.[1]). It was folded during the Hercynian orogeny and currently offers a world-class record of predominantly shallow-marine Cambrian to Carboniferous depositional sequences[1,2,3]. There, the Ordovician succession is up to 2 km in thickness. The Lower Palaeozoic succession is dominated by shallow-marine siliciclastics. During the latest Ordovician, offshore shales prevailed in the basin[4] (Bou Ingarf/Tazzarine area). They graded laterally at basin edge into shoreface to tidal facies, which migrated basinward during regressive events. Only in the middle-late Hirnantian, glaciomarine to fluvioglacial environments arose.

Lithofacies and interpreted depositional environments are shown for four sections distributed from the latest Ordovician basin edge to the basin centre of the central Anti-Atlas depositional trough. The two basin-edge sections on the left-hand side (**a**-**b**) specifically represent latest Ordovician stratigraphies in locations that do not show a subsequent glacial overdeepening event. The third log (**c**) specifically represents a synthetic section with superimposed glacial erosion surfaces, the depth of which is in fact deeper than illustrated, in the 75-200 m range (**f**). In this location, fully bioturbated shallow-marine intervals noticeably occur in between glacial erosion surfaces. The stratigraphic distribution of a pre-glacial, lower to middle Hirnantian, *Hirnantia or Hirnantia*-related fauna is shaded[1,5,6]. The section to the right (**d**) depicts a basin-axis location, within which the ice sheet arrived later. Here, three individual glacial erosion surfaces numbered 3 to 5 are documented[7], yet the glacial erosion surfaces 1, 2 and 6 are not observed (i.e., related ice fronts did not reach the basin centre, see **f**). The Ouzregui Beds[4], at the Katian/Hirnantian boundary, correlate to the Pernik Beds of the Prague Basin[7,8].

The late Katian to Hirnantian chitinozoan biozones[9] of the upper Ktaoua and lower and upper Second Bani formations are illustrated for the two main sections (unpublished data at basin edge; at the basin centre[4,10]). In the basin-edge section, " Upper Ktaoua " and " Lower Ktaoua " formation names are in brackets to indicate that they are not coeval with formations in the basin-centre type section; chitinozoans of the " Upper Ktaoua Fm. " in the basin-edge sections belong to the *elongata* Biozone (Hirnantian), while those of the Upper Ktaoua Fm. at the basin axis indicate the *merga* Biozone (latest Katian). As a consequence, the " Upper Ktaoua Fm. " at the basin-edge is coeval with the lower member of the Second Bani formation.

The lower diagram (**f**) tentatively illustrates the spatial and temporal distribution of glacial erosion surfaces numbered 1-6 that have been mapped out and correlated from the basin edge to the basin centre in the last ten years. Glacial surfaces are essentially amalgamated toward the basin edge, with the exception of deep downcuttings or palaeovalleys (mainly tunnel valleys[11]) and intervening successions progressively open basinward. Glacial erosion surfaces 1 and 2 have the smallest extent, as they have not been so far observed in the Bou Ingarf area[4,12] (BI). The Tizi n'Tazougart palaeovalley (TzT) has been illustrated before[1,13]. Glacial erosion surfaces 3 and 4 correspond to the Hirnantian glacial maxima and expand northward at least into the High Atlas, and at least one of the two reaches the Meseta area[14]. Glacial erosion surfaces 5 and 6 mark ice-sheet front readvances occurring during the overall deglaciation at the end of the Hirnantian, but may be only of regional significance. The glacial erosion surface 6 is associated with the tunnel valley known as the Foum Larjam palaeovalley (FoL [1,14]). The complexity generated by superimposed glacial erosion surfaces has been schematically accounted for in between the two sedimentary logs illustrated in the figure 2.

Above glaciation-related deposits, a *Hirnantia* fauna is preserved in places, which represents a postglacial recovery distinct from the earlier (shaded) *Hirnantia* fauna that predates the occurrence of glacial surfaces. Stratigraphic relationships at the transition from latest Ordovician to early Silurian strata are to some extent obscured by a Telychian unconformity. Rhuddanian strata (lowermost Silurian) have been documented overlying the Ordovician sandstones[1,15] in the area corresponding to the three most proximal sections. Conversely, at the basin axis, an erosional surface (transgressive surface) truncates the uppermost glaciation-related strata, which include cryogenic structures, and which are sealed by Telychian sandstones and shales of the *spiralis* graptolite Biozone[15,16].

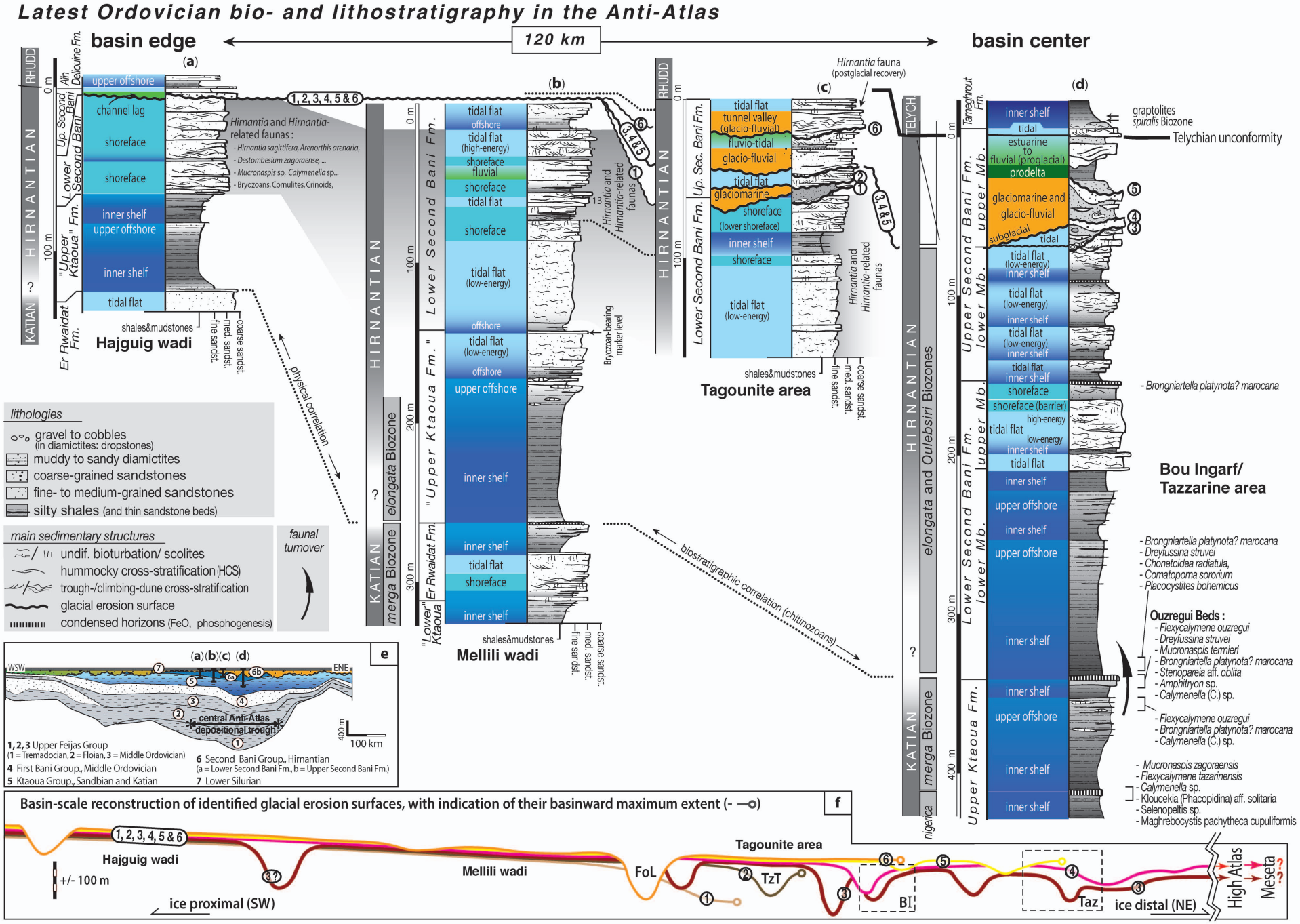
Latest Ordovician bio- and lithostratigraphy in the Anti-Atlas
basin edge
120 km
basin center
(a)
(b)
(c)
(d)
RHUDD
HIRNANTIAN
KATIAN
Up. Second Bani
Lower Second Bani Fm.
"Upper Ktaoua" Fm.
Er Rwaidat Fm.
Ain Dellouline Fm.
upper offshore
channel lag
shoreface
inner shelf
tidal flat
shales&mudstones
fine sandst.
med. sandst.
coarse sandst.
Hajguig wadi
Hirnantia and Hirnantia-related faunas :
- Hirnantia sagittifera, Arenorthis arenaria,
- Destombesium zagoraense, ...
- Mucronaspis sp, Calymenella sp...
- Bryozoans, Cornulites, Crinoids,
1, 2, 3, 4, 5 & 6
physical correlation
merga Biozone
elongata Biozone
tidal flat (high-energy)
fluvial
tidal flat (low-energy)
Bryozoan-bearing marker level
Mellili wadi
biostratigraphic correlation (chitinozoans)
Hirnantia fauna (postglacial recovery)
tidal flat tunnel valley (glacio-fluvial)
fluvio-tidal glacio-fluvial
glaciomarine
Tagounite area
TELYCH
Tamegroute Fm.
graptolites spiralis Biozone
Telychian unconformity
estuarine to fluvial (proglacial)
prodelta
glaciomarine and glacio-fluvial
subglacial
Bou Ingarf/ Tazzarine area
- Brongniartella platynota? marocana
- Dreyfussina struvei
- Chonetoidea radiatula,
- Comatopoma sororium
- Placocystites bohemicus
Ouzregui Beds :
- Flexycalymene ouzregui
- Dreyfussina struvei
- Mucronaspis termieri
- Brongniartella platynota? marocana
- Stenopareia aff. oblita
- Amphitryon sp.
- Calymenella (C.) sp.
- Flexycalymene ouzregui
- Brongniartella platynota? marocana
- Calymenella (C.) sp.
- Mucronaspis zagoraensis
- Flexycalymene tazarinensis
- Calymenella sp.
- Kloucekia (Phacopidina) aff. solitaria
- Selenopeltis sp.
- Maghrebocystis pachytheca cupuliformis
lithologies
gravel to cobbles (in diamictites: dropstones)
muddy to sandy diamictites
coarse-grained sandstones
fine- to medium-grained sandstones
silty shales (and thin sandstone beds)
main sedimentary structures
undif. bioturbation/ scolites
hummocky cross-stratification (HCS)
trough-/climbing-dune cross-stratification
glacial erosion surface
condensed horizons (FeO, phosphogenesis)
faunal turnover
e
WSW
ENE
central Anti-Atlas depositional trough
400 m
100 km
1, 2, 3 Upper Feijas Group (1 = Tremadocian, 2 = Floian, 3 = Middle Ordovician)
4 First Bani Group., Middle Ordovician
5 Ktaoua Group., Sandbian and Katian
6 Second Bani Group., Hirnantian (a = Lower Second Bani Fm., b = Upper Second Bani Fm.)
7 Lower Silurian
f
Basin-scale reconstruction of identified glacial erosion surfaces, with indication of their basinward maximum extent (- -o)
Hajguig wadi
+/- 100 m
ice proximal (SW)
Mellili wadi
FoL
Tagounite area
TzT
BI
Taz
ice distal (NE)
High Atlas
Meseta

Supplementary Figure 2

Bio-, litho-, and chemostratigraphy at Anticosti Island. The upper 900 m of the >2 km thick Sandbian to Telychian Anticosti succession (**a** and **d**) constitutes a comprehensive, latest Ordovician to early Silurian, record of thick, storm-dominated depositional sequences[17]. Mid to outer ramp carbonate facies that prevail in the western part of Anticosti Island grade eastward towards the basin margin into thinner, more siliciclastic-rich inner to proximal mid ramp facies that include several local discontinuities[18,19]. The first-order stratigraphic trends of this exposed succession display a long-term shelf aggradation from the late Katian to the early Telychian, culminating into a shelf progradation and basin fill due to the reduced post-Taconic tectonic subsidence during the Telychian. The shelf aggradation phase is, however, interrupted in the late Hirnantian by the presence of atypical shallow water limestones bounded by two regional disconformities extending far into the basin.

The late Katian to early Rhuddanian chitinozoan biozones[20] of the upper Vauréal, Ellis Bay, and lower Becscie formations are illustrated for the western (**b**) and eastern (**c**) sections of Anticosti Island. From the base of the Ellis Bay Formation to the base of the uppermost Laframboise Member at the west end of the island, three chitinozoan zones are distinguished in ascending order: the *florentini-concinna* Zone, the *gamachiana* Zone and the *taugourdeaui* Zone[19,21]. These zones are all considered Hirnantian in age, based on several concordant paleontological data related to the occurrence of pre- and post-extinction Hirnantian biota. This statement harmonizes with those previously reached on the basis of acritarchs[22], of brachiopods[23-29], of stromatoporoids[30], and of graptolites[31] (the black star in the West End section locates a graptolite assemblage identifying the N. *persculptus* Biozone). Other faunal groups display similar patterns including crinoids[32], nautiloids[33], and rugose corals (McLean and Copper, written commun. 2012). In the western section, the member names of the Ellis Bay Formation are in brackets to indicate that they are not coeval with their eponyms of the eastern section; as an example, chitinozoans of the Grindstone Member in the eastern section belong to the H. *crickmayi* Zone, while those of the "Grindstone Member" in the western section indicate the H. *florentini*-C. *concinna* Zone. As for the Anti-Atlas, revised chitinozoan biostratigraphy results in regional-scale correlations that are noticeably different from lithostratigraphic schemes. The lithostratigraphic framework of the latest Ordovician strata exposed on Anticosti Island is currently under revision (P. Copper, pers. commun. 2012).

Depositional facies at the highly subsiding western end of the island are dominated by mid- to outer-ramp, storm-dominated carbonates with calcareous shales[18,34]. Storm-influenced siliciclastic shoreface to mid ramp sediments prevail at the eastern end of the island. Oncolitic limestones associated with local metazoan-calcimicrobial reef development are present along the entire outcrop belt in the Laframboise Member of the uppermost Ellis Bay Formation[23].

Our high-resolution $\delta^{13}C$ curve (n= 135 micrites; (**a**) and Supplementary Table 1) extends from the Vauréal Formation up to the lower Becscie Formation at the west end of the island[35]. For the first 100 meters, $\delta^{13}C$ values are relatively stable and contain values of approximately 0 to 1 ‰, with a mean of 0.4 ‰ and a standard deviation of 0.25 ‰; the orange strip in (**a**) represents the 95 % confidence interval. These represent the background values for $\delta^{13}C$ prior to the very latest Katian. The Hirnantian age of the Ellis Bay Formation confirms that the Hirnantian isotopic carbon excursion (HICE) is not restricted to the main peak in the Laframboise Member, but includes the smaller excursions in the lower part of the formation and in the uppermost part of the Vaureal Formation. The $\delta^{13}C$ drops to pre-excursion values in the A. *ellisbayensis* chitinozoan zone at the base of the Becscie Formation during the uppermost N. *persculptus* Zone[19].

The Middle Ordovician to Llandovery portion of the surface and subsurface stratigraphy of the Anticosti Basin is illustrated in (**e**) (modified from Long[17]). The subsidence curve of the Anticosti succession shows periods of increased subsidence rates during the Sandbian-Katian and Aeronian that are related to Taconian and Salinic tectonic events further south in the Humber Zone and Gaspé Belt[36]. Coupled with a sustained sediment supply within the basin, the Anticosti record is exceptionally thick (e.g. Sandbian to Katian 1600 m, Hirnantian ~100 m, Rhuddanian to Telychian 500m), one or two orders higher than present in age equivalent carbonate sections of other shallow epeiric or ramp settings[37]. This argues against the proposition, based on chemostratigraphic analysis[38-41] that the Hirnantian and its associated HICE could be restricted to less than 10 m within the uppermost Ellis Bay Formation (see also Fig. 4 in the main text).

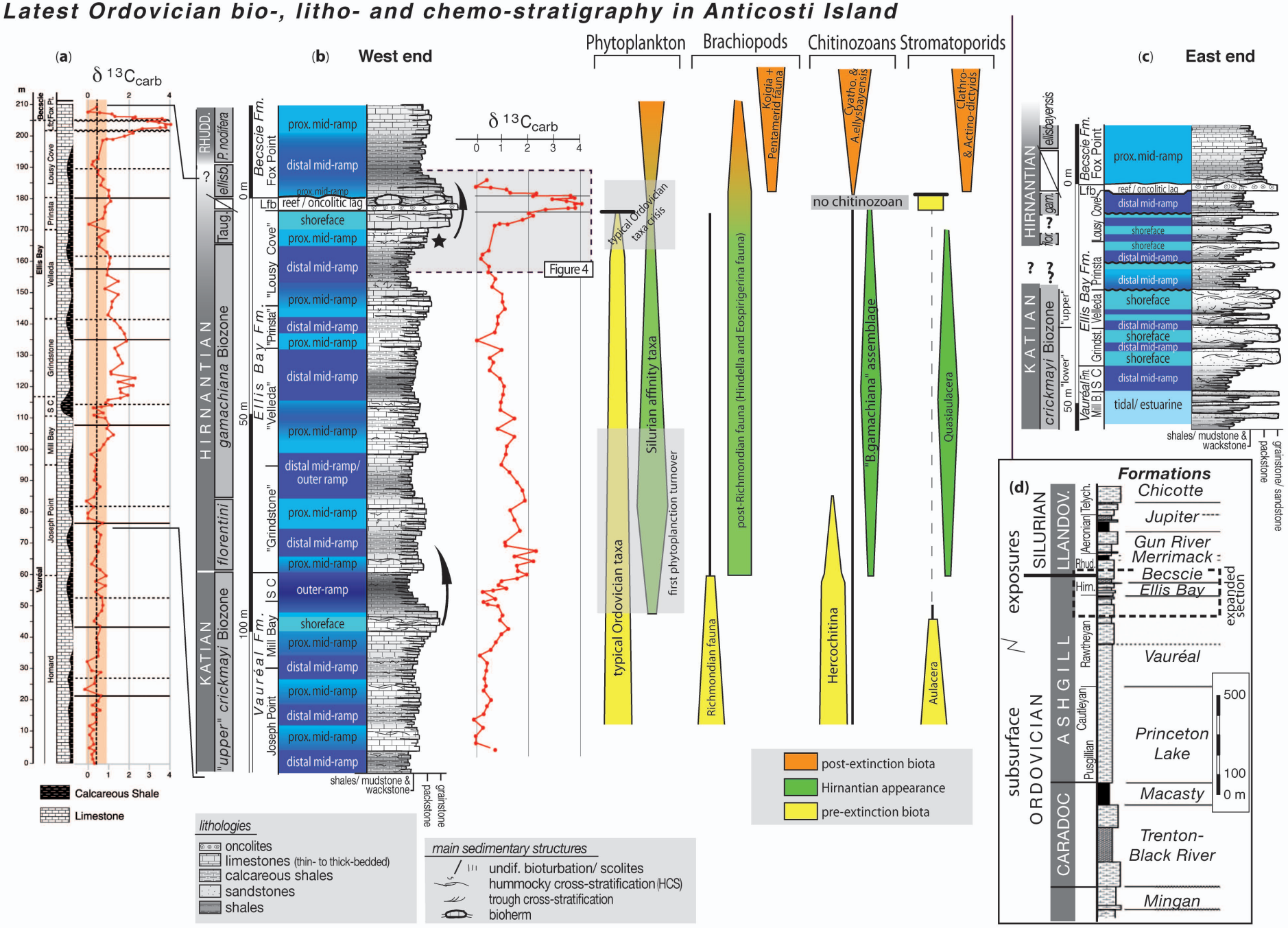
Latest Ordovician bio-, litho- and chemo-stratigraphy in Anticosti Island
(a)
δ 13Ccarb
(b) West end
(c) East end
Phytoplankton
Brachiopods
Chitinozoans
Stromatoporids
Figure 4
typical Ordovician taxa
Silurian affinity taxa
first phytoplanction turnover
post-Richmondian fauna (Hindella and Eospirigerina fauna)
Richmondian fauna
Kolgia + Pentamerid fauna
Cyatho. & A.ellysbayensis
Clathro- & Actino-dictyids
no chitinozoan
"B.gamachiana" assemblage
Hercochitina
Quasiaulacera
Aulacera
post-extinction biota
Hirnantian appearance
pre-extinction biota
Calcareous Shale
Limestone
lithologies
oncolites
limestones (thin- to thick-bedded)
calcareous shales
sandstones
shales
main sedimentary structures
undif. bioturbation/ scolites
hummocky cross-stratification (HCS)
trough cross-stratification
bioherm
shales/ mudstone & wackstone
packstone
grainstone
grainstone/ sandstone
(d)
Formations
Chicotte
Jupiter
Gun River
Merrimack
Becscie
Ellis Bay
Vauréal
Princeton Lake
Macasty
Trenton-Black River
Mingan
expanded section
subsurface
exposures
ORDOVICIAN
SILURIAN
CARADOC
ASHGILL
LLANDOV.
HIRNANTIAN
KATIAN
RHUDD.
Becscie Fm.
Fox Point
Lousy Cove
Ellis Bay Fm.
Prinsta
Velleda
Grindstone
Mill Bay
Joseph Point
Vauréal Fm.
Homard
Rawtheyan
Cautleyan
Pusgillian
Aeronian
Telych.
Rhud.
Hirn.
florentini
gamachiana Biozone
crickmayi Biozone
"upper"
"lower"
"Prinsta"
"Velleda"
"Grindstone"
"Lousy Cove"
prox. mid-ramp
distal mid-ramp
distal mid-ramp/ outer ramp
outer-ramp
shoreface
tidal/ estuarine
reef / oncolitic lag
Lfb
S C
50 m
100 m
500
100
0 m

Supplementary Figure 3

Stratigraphic sampling of shelf settings during glaciation. Conceptual models, based on Jervey's approach[42], illustrate relationships between the rates of relative base-level change (glacio-eustasy and subsidence), initial water depth and sediment supply for shelfal archives during icehouse conditions. The resulting stratigraphic columns in siliciclastic shelf environments after three scenarios are discussed below.

The glacio-eustatic forcing is based on the Quaternary glacial/interglacial model from Isotopic Stages 1 to 11. The relative sea-level in (**a**) includes a long-term subsidence-related component of 40 m for time interval under consideration, while no subsidence is assumed in (**b**) and (**c**). The green time intervals are times with corresponding depositional units, while the red segments represent hiatuses, the latter subaerial erosion surfaces or time-transgressive sedimentary condensations[43]. In (**a**), subsidence combined with moderate initial water depths (~ 100 m) and relatively high sediment supply result in ~42% stratigraphic sampling and 58% hiatuses. The initial glacio-eustatic oscillations (time intervals 11-7) are well represented in the depositional succession, while hiatuses (time intervals 6 and 4-2) correspond to most of the later lowstand events[44]. The resulting picture is that of high-frequency cycles, particularly from intervals with the greater sea-level highstands.

The scenario in (**b**) is as in (**a**), but without subsidence and with an initial water depth reduced to < 100 m. The outcome is a thin succession with a very low (<20%) stratigraphic sampling and multiple, severe, amalgamated hiatuses. Only the record of the earliest sea-level evolution is preserved despite abundant sediment supply. In contrast, for scenario (**c**), with a significant initial water depth of > 100 m, in general a deeper shelf beyond the shelf roll-over, the stratigraphic sampling is substantial, at ~60%; despite low sediment supply in this case, only the later glacio-eustatic lowstand events correspond to erosion surfaces. However, the resulting stratigraphic column is thin, with a poorly decipherable record.

For a given glacio-eustatic scenario, it is the rates of shelf subsidence, sediment supply, and initial depositional depths at glaciation onset that control sampling and temporal extent of stratigraphic units[45]. At any rate, stratigraphic hiatuses account for 40% to 80% of the time span in shelfal domains. Basin overfilling resulting in erosion and hiatuses is delayed when subsidence is active (**a**) or initial water depth is significant (**c**). Active subsidence results in a great number of depositional units and a representative record, providing the rate of sediment supply is adjusted to subsidence rates (**a**). Negligible or moderate subsidence rates (**b**), or great initial water depths (**c**), result in a limited number of well differentiated depositional units[44]: in (**b)**, depositional units essentially superimpose a set of discrete cycles; in (**c**), several low- to high-frequency cycles are amalgamated. Similar relationships are expected in carbonate platforms and all three scenarios are potentially applicable to the latest Ordovician case studies. Applied to the Hirnantian record, we suggest that the Anticosti Island stratigraphy resembles the (**a**)-type diagram. See also Permian—Carboniferous case studies[46,47].

For the glaciated shelf, contrasting records arise at outer and inner shelf settings (**d**). The outer shelf includes a pro- to inter-glacial stratigraphic record, generating sequences somewhat similar to the (**a-c**) scenarios (green parts) with hiatuses only at glacial maxima (in red). The inner shelf record, on the other hand, samples major interglacials, and most of the time is represented by erosion surfaces[48,49,50]. Interestingly, four glacial time intervals and related glacial erosion surfaces are captured in both cases, but they do not represent coeval glacial cycles. Clearly, the glaciated inner shelf record (e.g. Mauritania, Libya or Niger in the end-Ordovician[12,51,52]) is not correlatable in a one-to-one manner to depositional units of the far-field Anticosti Island stratigraphic sampler. The Anti-Atlas record that is understood as that of a glaciated outer shelf[12] is expected to correlate more closely with the Anticosti Island record, except at the time of glacial climax.

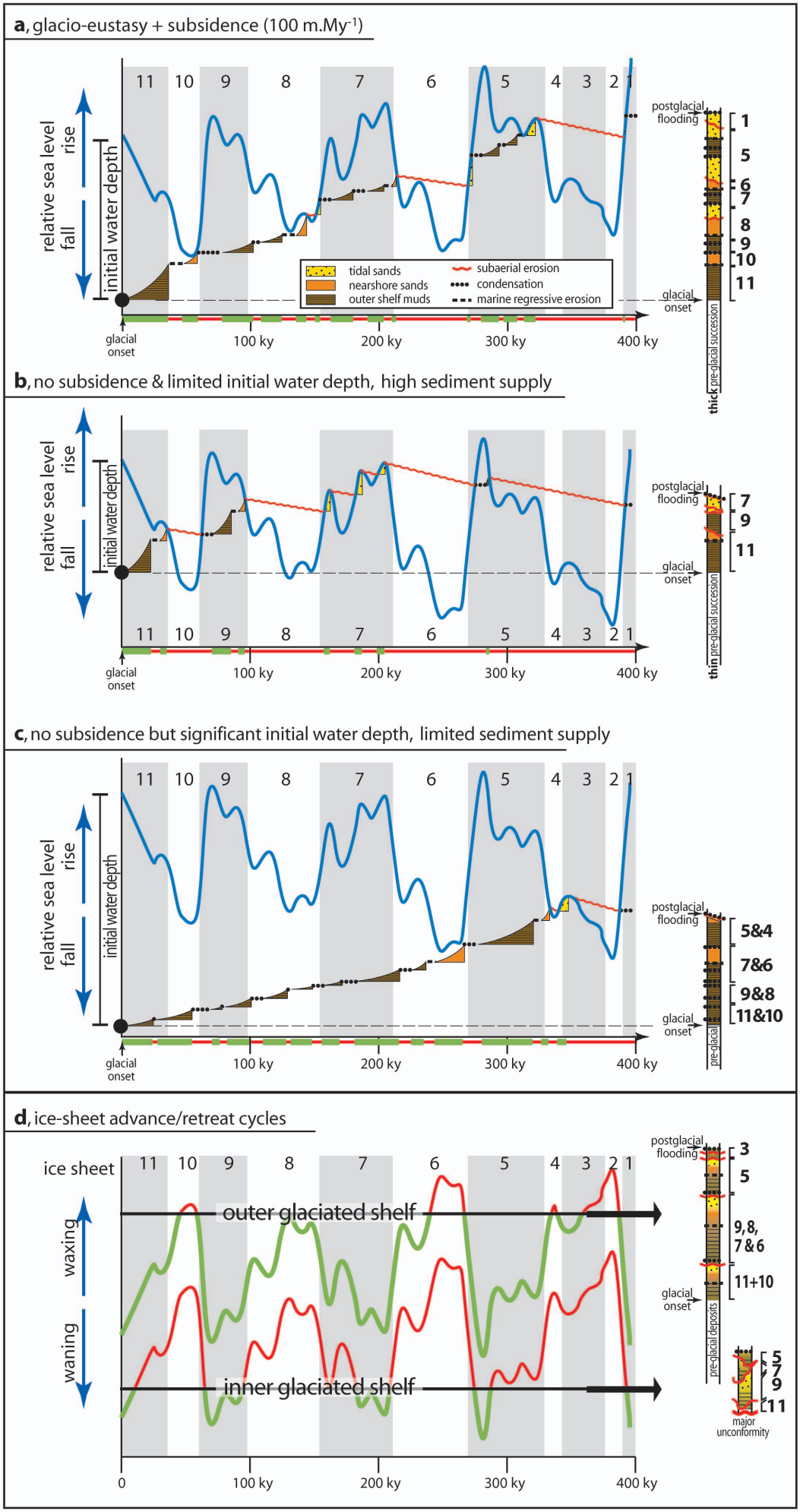
a, glacio-eustasy + subsidence (100 m.My-1)
relative sea level
rise
fall
initial water depth
11 10 9 8 7 6 5 4 3 2 1
tidal sands
nearshore sands
outer shelf muds
subaerial erosion
condensation
marine regressive erosion
glacial onset
100 ky
200 ky
300 ky
400 ky
postglacial flooding
glacial onset
pre-glacial succession
thick
1
5
6
7
8
9
10
11
b, no subsidence & limited initial water depth, high sediment supply
relative sea level
rise
fall
initial water depth
11 10 9 8 7 6 5 4 3 2 1
glacial onset
100 ky
200 ky
300 ky
400 ky
postglacial flooding
glacial onset
pre-glacial succession
thin
7
9
11
c, no subsidence but significant initial water depth, limited sediment supply
relative sea level
rise
fall
initial water depth
11 10 9 8 7 6 5 4 3 2 1
glacial onset
100 ky
200 ky
300 ky
400 ky
postglacial flooding
glacial onset
pre-glacial
5&4
7&6
9&8
11&10
d, ice-sheet advance/retreat cycles
ice sheet
11 10 9 8 7 6 5 4 3 2 1
waxing
waning
outer glaciated shelf
inner glaciated shelf
0
100 ky
200 ky
300 ky
400 ky
postglacial flooding
glacial onset
pre-glacial deposits
3
5
9,8,
7&6
11+10
5
7
9
11
major unconformity

Supplementary Table 1

$\delta^{13}C$ dataset from Katian to lowermost Silurian at the Anticosti Island. Stable isotope measurements were made on either micritic matrixes or the micritic phase of pelloids in grainstone facies[35]. Some samples were analyzed more than once: "QCD" indicates a Quality Control Duplicate, which is used to test the accuracy of the mass spectrometer, "repeat" denotes a sample that was analyzed again due to it being an anomalous measurement, or having encountered a problem in the process of measurement. The data are listed relative to the PDB standard. Sampled section 1A, West End (Baie St. Claire – Laframboise Section); its base is in the "Homard" Member of the Vaureal Formation; it spans the entire Ellis Bay Formation, and terminates in the lower Fox Point Member of the Becscie Formation.

Sample #	Height (m)	Description	$\delta^{13}C$ (‰)	$\delta^{18}O$ (‰)
B-M-01	0	mudstone/packstone	0.3	-3.22
B-M-02	1.33	wackestone/packstone	0.24	-2.98
B-M-03	2.66	wackestone/packstone	0.18	-3.15
B-M-03 QCD	2.66	wackestone/packstone	0.16	-3.35
B-M-04	4	wackestone/packstone	0.32	-2.74
B-M-05	5.33	wackestone/packstone	0.05	-4.05
B-M-06	6.66	mudstone/packstone	0.26	-3
B-M-07	8	wackestone	0.2	-3.11
B-M-08	9.33	wackestone	0.07	-3.92
B-M-09	10.66	packstone	0.26	-3.68
B-M-10	12	mudstone/wackestone	0.08	-4.07
B-M-11	13.33	wackestone/packstone	0.4	-4.34
B-M-12	14.66	mudstone/packstone	0.41	-4.25
B-M-13	16	mudstone/wackestone	0.23	-4.66
B-M-13 QCD	16	mudstone/wackestone	0.26	-4.64
B-M-14	17.33	mudstone	0.59	-4.27
B-M-15	18.66	mudstone/wackestone	0.22	-4.32
B-M-16	20	mudstone/wackestone	0.49	-3.83
B-M-17	21.8	wackestone	0.66	-5.01
B-M-18	23.6	mudstone/wackestone	-0.18	-4.74
B-M-19	25.4	wackestone	0.32	-4.83
B-M-20	27.3	wackestone/packstone	0.35	-4.13
B-M-21	29.1	wackestone/packstone	0.63	-4.02
B-M-22	29.9	packstone	0.18	-3.88
B-M-23	32.7	packstone	-0.03	-4.13
B-M-24	34.6	wackestone	0.51	-4.45
B-M-24 QCD	34.6	wackestone	0.48	-4.47
B-M-25	36.4	wackestone	0.49	-4.13
B-M-26	38.2	mudstone/wackestone	0.52	-3.87
B-M-27	40	wackestone	0.43	-4.74
B-M-28	41.8	wackestone	1.53	-1.68
B-M-28 repeat	41.8	wackestone	1.75	-1.47
B-M-29	43.6	mudstone/wackestone	0.6	-3.42
B-M-30	45.4	mudstone/wackestone	0.3	-4.12
B-M-31	47.3	mudstone/wackestone	0.46	-4.48
B-M-32	49.1	wackestone	0.7	-4.26

B-M-33	49.9	wackestone/packstone	0.7	-3.64
B-M-33 QCD	49.9	wackestone/packstone	0.72	-3.96
B-M-34	52.7	mudstone/wackestone	0.68	-4.05
B-M-35	54.6	packstone	0.36	-4.23
B-M-36	56.4	mudstone/packstone	0.85	-3.58
B-M-37	58.2	wackestone	0.39	-3.83
B-M-38	60	wackestone/packstone	0.88	-3.48
B-M-39	61.8	mudstone/wackestone	0.58	-4.34
B-M-40	63.6	wackestone	0.15	-3.94
B-M-41	65.4	wackestone	0.37	-3.65
B-M-42	67.3	mudstone/wackestone	0.48	-3.53
B-M-43	69.1	wackestone/packstone	0.38	-4.18
B-M-43 QCD	69.1	wackestone/packstone	0.36	-4.18
B-M-44	69.9	mudstone/wackestone	0.52	-3.65
B-M-45	72.7	mudstone/packstone	0.62	-3.36
B-M-46	74.6	mudstone/packstone	0.32	-3.57
B-M-47	76.4	wackestone/packstone	0.71	-4.26
B-M-48	78.2	wackestone/packstone	0.01	-3.85
B-M-49	80	mudstone/wackestone	-0.01	-4.23
B-M-50	81.66	wackestone/packstone	0.28	-3.72
B-M-51	83.33	mudstone/wackestone (stylolitic)	-0.07	-4.62
B-M-52	85	mudstone/wackestone	0.29	-3.43
B-M-53	86.66	mudstone	0.44	-3.68
B-M-53 QCD	86.66	mudstone	0.43	-3.65
B-M-54	88.33	mudstone	0.57	-3.76
B-M-55	90	mudstone	0.3	-3.71
B-M-56	91.66	mudstone/wackestone	0.36	-3.62
B-M-57	93.33	mudstone/wackestone	0.33	-3.69
B-M-58	95	wackestone	0.4	-3.82
B-M-59	96.66	wackestone	0.45	-3.66
B-M-60	98.33	wackestone	0.16	-3.97
B-M-61	100	mudstone (stylolitic)	0.55	-3.45
B-M-62	101.66	mudstone	0.78	-3.46
B-M-63	103.33	mudstone/wackestone	0.97	-2.89
B-M-63 QCD	103.33	mudstone/wackestone	1	-2.9
B-M-64	105	wackestone/packstone	1.22	-3.02
B-M-65	106.66	mudstone/wackestone	0.93	-3.08
L-M-01	100	packstone (brachiopod)	0.8	-3.46
L-M-02	102.5	wackestone/packstone	0.71	-3.26
L-M-03	105	wackestone	1.06	-4.58
L-M-04	107.5	packstone	1.01	-3.21
L-M-05	110	packstone	0.84	-3.36
L-M-06	110.6	packstone	0.44	-3.76
L-M-07	111.1	packstone (brachiopod)	0.25	-3.13
L-M-08	111.7	wackestone/packstone	0.76	-3.04
L-M-08 QCD	111.7	wackestone/packstone	0.74	-2.99
L-M-09	112.2	packstone	0.61	-3.22
L-M-10	112.8	wackestone/packstone	0.98	-3.04
L-M-11	113.3	wackestone	0.26	-3.43
L-M-12	113.9	packstone	0.66	-3.33
L-M-13	114.4	packstone	1.16	-3.48
L-M-14	115	packstone/grainstone	0.85	-3.89

L-M-15		115.83	packstone	0.98	-3.67
L-M-16		116.66	packstone	1.61	-3.04
L-M-17		117.5	grainstone (peloidal)	1.94	-3.13
L-M-18		118.33	packstone	1.59	-3.44
L-M-18	QCD	118.33	packstone	1.61	-3.42
L-M-19		119.16	packstone	1.6	-3.24
L-M-20		120	packstone	0.28	-3.25
L-M-21		120.83	wackestone	2.26	-3.26
L-M-22		121.66	wackestone	1.47	-3.66
L-M-23		122.5	wackestone	2.36	-3.18
L-M-24		123.33	mudstone	2.35	-3.02
L-M-25		124.16	packstone	1.17	-3.55
L-M-26		125	packstone	1.1	-3.96
L-M-27		127.5	wackestone/packstone	1.69	-3.49
L-M-28		130	packstone	1.44	-3.5
L-M-28	QCD	130	packstone	1.51	-3.48
L-M-29		132.5	wackestone/packstone	1.32	-3.14
L-M-30		134.6	wackestone	1.9	-3.28
L-M-31		136.7	mudstone/wackestone	1.78	-3.32
L-M-32		138.8	mudstone/wackestone	1.56	-3.43
L-M-33		140.9	wackestone	1.29	-3.26
L-M-34		143	wackestone	0.98	-3.15
L-M-35		145.1	wackestone	1.15	-3.48
L-M-36		147.2	wackestone	1.19	-3.25
L-M-37		149.3	mudstone/wackestone	1.47	-3.15
L-M-38		151.4	wackestone	0.81	-3.28
L-M-38	QCD	151.4	wackestone	0.85	-3.29
L-M-39		153.5	mudstone	1.46	-3.36
L-M-39 repeat		153.5	mudstone	1.54	-3.75
L-M-40		155.6	mudstone/wackestone	0.95	-3.34
L-M-41		157.4	mudstone	0.95	-3.46
L-M-42		159.2	wackestone	1.04	-3.45
L-M-43		161	wackestone/packstone	1.08	-3.4
L-M-44		162.8	wackestone	0.9	-3.28
L-M-45		164.6	wackestone/packstone	0.54	-3.38
L-M-46		166.4	wackestone/packstone	0.66	-3.31
L-M-47		168.2	packstone	0.5	-3.73
L-M-48		170	wackestone	0.99	-3.51
L-M-49		171.8	wackestone	0.02	-3.18
L-M-50		173.6	mudstone/wackestone	0.72	-3.32
L-M-50	QCD	173.6	mudstone/wackestone	0.72	-3.34
L-M-51		175.4	mudstone/wackestone	0.82	-3.14
L-M-52		177.2	wackestone	0.84	-3.26
L-M-53		179	wackestone	1.11	-3.9
L-M-54		180.8	wackestone	1.04	-3.65
L-M-55		182.6	wackestone	1.02	-3.62
L-M-56		184.4	wackestone	0.62	-4.58
L-M-57		186.2	packstone	0.74	-3.88
L-M-58		188	packstone	0.49	-3.47
L-M-59		188.9	wackestone/packstone	0.47	-3.61
L-M-59	QCD	188.9	wackestone/packstone	0.55	-3.53
L-M-60		189.8	wackestone/packstone	0.29	-3.52

L-M-61	190.7	wackestone/packstone	0.2	-3.71
L-M-62	191.6	wackestone/packstone	0.26	-3.83
L-M-63	192.4	packstone (brachiopod)	0.47	-3.81
L-M-64	193.3	packstone	0.52	-4.06
L-M-65	194.2	packstone	0.69	-3.4
L-M-66	195.1	packstone	0.94	-3.1
L-M-67	196	wackestone/packstone	1.99	-3.03
L-M-68	197.5	mudstone	1.95	-3.71
L-M-69	199	mudstone/wackestone	1.93	-3.69
L-M-70	201	wackestone	1.92	-3.92
PL-4i	197.5	Peloidal grst/pakst	1.80	-2.75
PL-5i	198	Peloidal grst/packst	1.84	-3.12
PL-6i	198.5	Peloidal grst/packst	2.20	-3.53
PL-7i	199	Peloidal grst/packst	2.27	-3.42
PL-8i	200	Peloidal grst/packst (top Lousy Cove)	2.05	-3.87
PL-9i	200.5	Oncolitic packst/grst (base Laframboise)	2.69	-3.46
PL-10i	200.9	Oncolitic packst/grst	3.56	-2.73
PL-11i	201.1	Oncolitic packst/grst	3.85	-2.38
PL-12i	201.5	Oncolitic packst/grst	4.04	-2.74
PL-13i	201.8	Oncolitic packst/grst	3.78	-2.88
PL-14i	202.1	Oncolitic packst/grst	3.48	-2.69
PL-15i	202.8	Inter-reef wackst/packst	2.95	-2.96
PL-16i	203.2	Inter-reef wackst/packst	3.85	-2.75
PL-17Bi	203.8	Inter-reef wackst/packst	3.60	-2.85
PL-18i	204.1	Inter-reef wackst/packst (top Laframboise)	3.63	-2.28
PL-19Ai	204.3	packstone-wackestone (base Becscie)	2.18	-4.39
PL-20i	204.5	packstone-wackestone	2.31	-4.36
PL-21i	204.8	packstone-wackestone	1.49	-3.64
PL-22i	205.3	wackestone	1.16	-3.15
PL-23i	205.6	wackestone	1.18	-3.08
PL-24i	205.9	wackestone	0.58	-3.99
PL-25i	206.2	wackestone	0.56	-3.34
PL-26i	206.5	wackestone	0.00	-4.24
PL-27i	207.5	wackestone	0.42	-3.80
PL-28i	208.5	wackestone	0.34	-3.69

Supplementary Table 2

Reservoirs of the Ordovician–Silurian global carbon cycle. Estimated quantities of the reservoirs of the Ordovician–Silurian global carbon cycle[35]. With flux quantities (Supplementary Table 3), these are the basis for the box model presented in the Supplementary Discussion.

Reservoir	abbr.	Gt C (today)	Gt C (O-S)	$\delta^{13}C$ (‰)
Lithosphere	l	150,000,000	69,802,795	-6
Carbonates	c	70,000,000	150,000,000	0
Fossil Fuels	f	20,000	10,000	-28
Reactive Sediments	r	3,000	18,000	0
Deep Ocean	d	38,000	220,000	0
Surface Ocean	s	1,000	6,000	+3
Phytomass	p	500	5	-28
Soil		2500	0	
Atmosphere	a	800	9,000	-6

Supplementary Table 3

Fluxes of the Ordovician–Silurian global carbon cycle. Estimated quantities for the fluxes of the Ordovician–Silurian global carbon cycle[35]. With reservoir quantities (Supplementary Table 2), these are the basis for the box model presented in the Supplementary Discussion.

Flux	abbr.	Gt/yr (today)	Gt/yr (O-S)
Terrestrial primary production	a → a	63.1	0
Marine primary production	a → a	50.5	80
Volatilization from soil	a → a	62.5	0
CO_2 dissolution & evasion	a → a	96	1050
$CaCO_3$ production & dissolution	s → s	0.5	0.5
CO_2 uptake by plants & humus	a → p	0.6	0
CO_2 used in weathering	a → l	0.26	0.13
River input from silicates	l → s	0.25	0.13
River input from carbonates	c → s	0.13	0.06
River input from organic matter	c → s	0.31	0
Ocean-atmosphere exchange	s → a	0.48	0
$CaCO_3$ storage in sediments	s → c	0.38	0.38
Organic C storage in sediments	s → c	0.1	0.1
Upwelling	d → s	2.15	12.5
Volcanism & metamorphism	l → a	0.12	0.18
Hydrothermal	l → a	0.1	0.15
Uplift	l → a	0.4	0.4

Supplementary Note

The essentials of the three Late Ordovician Glacial Cycles (LOGCs)

We here summarize the essentials that characterize the three Late Ordovician Glacial Cycles, as understood from the high-resolution sequence stratigraphic frameworks (Figure 2), in the near-field Anti-Atlas (Supplementary Fig. 1) and the far-field Anticosti Island (Supplementary Fig. 2).

Anti-Atlas

LOGC 1 includes a severe latest Katian sea-level fall reflected by a major facies shift at the basin edge and an ensuing important transgression with basin-wide sediment starvation and condensation in the very latest Katian. Maximum regressive and early transgressive facies together form the Ouzregui Beds[4], coeval with a significant faunal turnover, corresponding to the replacement of the diversified Late Katian faunas by a poorly diversified *Hirnantia*-related fauna, which is only present at basin edges, and not in deeper parts of the depocentre.

The lower to middle Hirnantian LOGC 2 commences with a highstand. Then, two high-order GSS with strikingly sharp-based, regressive depositional units, characterize its lower part. The older GSS is poorly developed in basinal position, while the younger one is best recognized in the basin centre. No subaerial exposure occurred at this time at the basin centre, but is suspected at the basin edge. Associated significant sedimentary aggradation suggests that this regressive succession is a lowstand wedge reflecting early time-transgressive conditions immediately following the glacial maximum of LOGC2. A relatively long-term transgressive trend followed that included well-defined higher-order oscillations capped by a major flooding surface with phosphogenesis.

The late Hirnantian LOGC 3 is essentially preserved at the basin axis, and/or within restricted glacially-related overdeepenings (Supplementary Fig. 1). Thin regressive nearshore facies ascribed to falling stage deposits are truncated by a glacial wedge (the glacial interval in Fig. 2) that includes several polyphased glacial erosion surfaces and related glaciomarine to fluvioglacial units. Within the glacial wedge, glacio-eustatic cycles are difficult to decipher because glacio-eustasy here is expected to have interfered with glacio-isostasy. The subsequent post-glacial transgression is associated with renewed deposition at the basin margin, re-colonisation by a *Hirnantia* fauna, and a severe latest Hirnantian to Rhuddanian condensation[1]. In the basin centre, an early Silurian unconformity of unknown origin associated with a ca. 7 myr long hiatus truncates the very latest deglacial Ordovician record[16].

The first-order stratigraphic trends reveal a long-term shelf progradation through the latest Katian to the late Hirnantian, which was punctuated by multi-order regressive and/or glacial events. The Hirnantian glacial record included in LOGC 3 is only preserved in a lowstand, basinal position, with virtually no record (except in glacial overdeepenings) at the basin edge. Post-glacial flooding was non-accretionary[53], suggesting high rates of sea-level rise in the very latest Hirnantian.

The glacial record (glacial erosion surface, glaciotectonic deformation, tunnel channels, ice-contact deposits) of LOGC 1 is known in Niger[51] as re-interpreted in Loi et al.[4], while that of LOGC 2 and 3 most likely correspond to the well known glacial successions in Libya, Algeria and Mauritania[12,52,54-59].

Anticosti Island

Several orders of depositional units, reflecting multi-order base-level changes, were identified in the Anticosti succession that display striking similarities with the time-equivalent Anti-Atlas sequence. During the latest Katian LOGC 1, a major sea-level fall was followed by a significant transgressive event. This event, together with the ensuing highstand in the latest part of the Katian, is associated with a faunal turnover during which Katian acritarchs, chitinozoans, conodonts, brachiopods, nautiloids, crinoids, stromatoporoids, and corals are replaced by taxa with either Hirnantian or Silurian affinities. The first perturbation in a long-lived relatively stable Katian $\delta^{13}C$ signal coincide with late regressive conditions in the latest Katian (Mill Bay), and not with the earlier sea-level fall (Joseph Point; Fig. 3 and Supplementary Fig. 2). Two sharp-based, regressive units representing sea-level drops are well expressed in the western distal basin sections during the early-middle Hirnantian LOGC 2. The older one, characterized by a greater facies offset than the younger one, is associated with a basal regressive surface of marine erosion resulting in a stratigraphic hiatus during the lowermost Hirnantian. Subaerial exposure did not occur at that time at the basin centre, but was present at the basin margin. The $\delta^{13}C$ values are typically above the Katian background with a positive 2‰ excursion recorded above the first sharp-based surface. A well-expressed transgressive trend with higher-order oscillations is capped by a major flooding surface in the upper LOGC 2. This flooding event marks a return to typical Katian $\delta^{13}C$ values.

The middle-late Hirnantian LOGC 3 is composed of three distinct stratigraphic packages separated by two regional disconformities. The oldest package is a sharp-based regressive unit representing a major sea level drop. Its capping erosive surface recorded an emersion that was smoothed by ravinement during the ensuing transgression (see Fig. 4). This regressive unit coincides with a progressive increase in $\delta^{13}C$ values, up to +2‰. A second faunal turnover is recognized following the deposition and subsequent emersion of this initial package. This second turnover shows a more abrupt replacement of acritarchs, chitinozoans, conodonts, brachiopods, and corals than the first turnover, with the rapid disappearance of "Ordovician" taxa. The next package is composed of transgressive oncolitic calcirudites overlain locally by "keep-up" metazoan-calcimicrobial bioherms. The upper contact of the bioherms is erosional has local relief up to 10 m, and has a multi-phase origin including an initial emersion, a subsequent modification by a transgressive ravinement, and a final pyritic hardground development. The highest positive $\delta^{13}C$ values, up to 5‰ in places, are present in this middle package. The third package, locally onlaps and abuts against the exhumed massive bioherm cores of the underlying package. It displays a thin transgressive record at the more subsiding basin centre, but contains thicker, slightly older proximal ramp facies at the basin margin. This final package marks the return of pre-Hirnantian shelf aggradation architecture and displays a relatively rapid negative isotopic shift with return to $\delta^{13}C$ background values. The late Hirnantian LOGC-3 glacial far-field record is partially preserved at the basin centre, but reduced at the basin edge.

Within LOGCs 1 and 2, the $\delta^{13}C_{carb}$ curve rises during the late and early regressive system tracts (lowstand and highstand conditions, respectively) and declines during transgressive and late regressive system tracts, respectively. Note that within LOGC 2, the excursion encompasses several higer-order stratigraphic cycles. The third and greatest excursion recorded in LOGC 3 amalgamates two signals, one predating and one postdating the LOGC 3 glacial maximum that is

represented by the unconformity at the base of the Laframboise Mb. These are time-regressive and time-transgressive, respectively (Fig. 4).

The two time intervals that correspond to the first and second faunal turnovers are not restricted to two short-term "extinction" events, supposedly glacial onset and termination, respectively. In fact, the first turnover is essentially coincident with the first interglacial that separates LOGCs 1 and 2. The ensuing lowermost Hirnantian stratigraphic hiatus in the Anticosti Island succession is likely responsible for its apparent sharpness (Fig. 3). The second turnover includes the entire glacial maximum of LOGC 3, commencing during the glacio-eustatic regression and terminating during the early deglaciation phase.

Supplementary Discussion

Box model of the late Ordovician carbon cycle

A variety of models have been proposed to explain the large isotopic excursion(s) in the Hirnantian; the productivity hypothesis, the weathering hypothesis and changes in oceanic circulation pattern. These are successively examined below, in the light of a box model for the Late Ordovician global carbon cycle[35], with the conclusion that none of them can account for the amplitude of the observed anomaly at the global scale.

Presented here is a model designed to simulate the global carbon cycle for the Late Ordovician world. It is based mostly on the work of Mackenzie and Lerman[60], a review of hundreds of scientific studies of the past and present carbon cycling. This overview quantifies carbon reservoirs and fluxes on global scales. The Ordovician-Silurian carbon cycle, based on Mackenzie and Lerman's model, uses high Ordovician pCO_2 values (~4000 ppm) and also takes into account minimal vascular land-plant cover. This model can be used to test some of the theoretical aspects of the hypotheses concerning the $\delta^{13}C$ excursions that occurred near the O-S Boundary. The estimated quantities of the reservoirs and the fluxes of the Ordovician-Silurian global carbon cycle are given in Supplementary Table 2 and Supplementary Table 3, respectively.

In this simplified model, the relationships between various reservoirs, fluxes and isotope values of carbon are described by the conservation of mass

$$\Delta M_x/\Delta t = \underbrace{\Sigma F_{i\text{-}x}}_{\text{flux in}} - \underbrace{\Sigma F_{x\text{-}i}}_{\text{flux out}} \qquad (1)$$

and a similar equation involving the enrichment of organic carbon.

$$\Delta(M_x*\delta_x)/\Delta t = \underbrace{\Sigma F_{i\text{-}x}*\delta_i - \Sigma F_{x\text{-}i}*\delta_x}_{\text{inorganic carbon}} + \underbrace{\Sigma F_{i\text{-}x}^{\circ}*(\delta_i+\varepsilon) - \Sigma F_{x\text{-}i}^{\circ}*(\delta_x+\varepsilon)}_{\text{organic carbon}} \qquad (2)$$

Using the product rule and the two equations above we arrive at the equation of isotope continuity.

$$\Delta\delta_x/\Delta t = [\Sigma F_{i\text{-}x}*(\delta_i-\delta_x) + \Sigma F_{i\text{-}x}^{\circ}*(\delta_i+\varepsilon) - \Sigma F_{x\text{-}i}^{\circ}*(\delta_x+\varepsilon)] / M_x \qquad (3)$$

Where:
M_x represents the mass of C in a reservoir
$F_{i\text{-}x}$ is the flux of C from reservoir i into reservoir x
$F_{x\text{-}i}^{\circ}$ is the flux of organic C from reservoir x to reservoir i
δ_x is the isotopic value of a carbon reservoir
ε is the depletion factor for organic carbon

M_s = 6000 Gt	ε = –28 ‰
$F_{l\text{-}s}$ = 0.13 Gt/yr	δ_a = -6 ‰
$F_{c\text{-}s}$ = 0.06 Gt/yr	δ_l = -6 ‰
$F_{d\text{-}s}$ = 12.5 Gt/yr	δ_c = 0 ‰
$F_{s\text{-}a}$ = 0 Gt/yr	δ_c° = -28 ‰
$F_{s\text{-}c}$ = 0.38 Gt/yr	δ_d = 0 ‰
$F_{s\text{-}c}^{\circ}$ = 0.1 Gt/yr	δ_s = +3 ‰

In the case of the *global productivity hypothesis*, a change in the rate of burial of organic carbon, $F_{s\text{-}c}°$, brought the $\delta^{13}C$ of the surface ocean from 0 to 4 ‰, in the timespan of approximately 100,000 to 500,000 years.

$$\Delta\delta_s * M_s / \Delta t = F_{l\text{-}s} * (\delta_l - \delta_s) + F_{c\text{-}s} * (\delta_c - \delta_s) + F_{d\text{-}s} * (\delta_d - \delta_s) - F_{s\text{-}c}° * (\delta_s + \varepsilon) \quad (4)$$

$$+4\ ‰ * 6000\ Gt/\Delta t = 0.13\ Gt/yr * (-6\ ‰ - 3\ ‰) + 0.06\ Gt/yr * (0\ ‰ - 3\ ‰) + 12.5\ Gt/yr * (0\ ‰ - 3\ ‰) - F_{s\text{-}c}° * (3\ ‰ - 28\ ‰)$$

$$24{,}000\ ‰Gt / \Delta t = (-39\ ‰Gt/yr + 25\ ‰ * F_{s\text{-}c}°)$$

For the lower limit, Δt = 100,000 yr, $F_{s\text{-}c}°$ = 1.564 Gt/yr
For the upper limit, Δt = 500,000 yr, $F_{s\text{-}c}°$ = 1.556 Gt/yr

Therefore, to produce a $\delta^{13}C$ increase of 4 ‰ in the surface ocean, the carbon burial rate has to increase to approximately 1.56 Gt/yr, 15 times the present day rate of carbon burial in the oceans (0.1 Gt/yr); an unsustainable proposition on a global scale.

Cramer and Saltzman's hypothesis[61,62] for ocean state changes, the value for $F_{d\text{-}s}$, which represents upwelling of inorganic carbon from the deep ocean to the surface ocean, will have to change from 12.5 Gt/yr to 0, assuming stratified oceans with no active thermohaline circulation. This is difficult to conceive on a global scale but can be easily achieved on regional (basinal) scales.

$$+4\ ‰ * 6000\ Gt/\Delta t = 0.13\ Gt/yr * (-6\ ‰ - 3\ ‰) + 0.06\ Gt/yr * (0\ ‰ - 3\ ‰) + 0\ Gt/yr * (0\ ‰ - 3\ ‰) - F_{s\text{-}c}° * (3\ ‰ - 28\ ‰)$$

$$24{,}000\ ‰Gt / \Delta t = (-1.35\ ‰Gt/yr + 25\ ‰ * F_{s\text{-}c}°)$$

Δt = 100,000 yr, $F_{s\text{-}c}°$ = 0.064 Gt/yr
Δt = 500,000 yr, $F_{s\text{-}c}°$ = 0.056 Gt/yr

Therefore, a $\delta^{13}C$ increase of 4 ‰ in the surface ocean is possible with modern day burial rates of organic carbon but only on regional scales and providing the upwelling of water from the deep ocean were to cease completely. Considering that the tide-related recirculation of deep, dense water masses to the surface ocean is enhanced during lowstand events[63], such circumstances are in fact unlikely.

Note that in the Late Ordovician world, organic carbon was produced exclusively in the Surface Ocean Reservoir. Taking the above qualifications into account, let us now consider the viability of these earlier advocated Late Ordovician scenarios in the context of geological framework.

1) The *productivity hypothesis*[64] argues that phytoplankton blooms resulted in preferential removal of ^{13}C from the water column, leading to a drawdown of atmospheric CO_2 that initiated the Hirnantian glaciation, sea level drop, and generation of a widespread anoxia followed by the late Ordovician extinction event. The above model calculations[35] show, however, that the rate of organic carbon burial would have to be 15 times that of its modern counterpart and sustained over 10^7–10^8 years. This is an unrealistic proposition, even leaving aside the issue of the fate of the "missing" carbon-rich sediments in coeval sedimentary sections. This could have been a

viable scenario only if applied to localized basins within the broad epeiric seas of the Ordovician that may not have been strictly synchronous.

2) The alternative "*weathering" hypothesis* and its modifications[65-67] attributes the glaciation to CO_2 drawdown initiated by enhanced silicate weathering related to the Taconic Orogeny. The erosion of platform carbonates subsequent to glacially-induced sea-level fall is then advocated as an explanation for the HICE. The "weathering" scenario requires as a starting assumption riverine flux of carbon that is significantly depleted in ^{13}C. Such isotopically depleted carbon is presently derived from soil CO_2 that originates from decomposition of land-based biomass. The positive carbon excursion in the ocean is then driven by diminution of the input from such sources. Yet, the land-based biosphere prior to Silurian was either absent or putative and the input from soil CO_2 into the riverine systems has therefore been limited. At that time the dissolution of carbonates must have been dominated by carbonic acid derived mostly from ingassing of atmosperic CO_2 and the isotope signal of the riverine carbon flux would have been around 0 ‰. Moreover, the presumed additional erosional source associated with low sea levels, the underlying Paleozoic rocks, have $\delta^{13}C$ depleted (0–1 ‰)[68] relative to HICE and thus cannot be the cause of the anomaly. The onset of $\delta^{13}C$ excursions during regressive time intervals thus cannot be the consequence of enhanced erosion of platform carbonates, unless a significant land cover (and related massive production of carbonic acid) can be demonstrated in the Ordovician.

3) Another alternative argues that the sea level and/or climate triggered *changes in circulation patterns* [61,62,69-71], from upwelling dominated shelf circulations during highstands to downwelling during lowstand, resulted in redox stratification with a ^{13}C-rich upper layer due to enhanced productivity and a ^{13}C-depleted water body at depth. This hypothesis, in essence developed for Silurian $\delta^{13}C$ excursions, suffers the same limitations as (1) described above. It cannot be produced and sustained on the scale of global oceans. This scenario is feasible only for excursions developed on a basin scale during highstand conditions of a high-order GSS (see Fig. 4).

Supplementary References

1. Destombes, J., Hollard, H. & Willefert, S. Lower Palaeozoic rocks of Morocco. In *Lower Palaeozoic of North-western and West Central Africa* (ed C.H. Holland) 91–336 (John Wiley, New-York, 1985).
2. Burkhard, M., Caritg, S., Helg, U., Robert-Charrue, C. & Soulaimani, S. Tectonics of the Anti-Atlas of Morocco. *C.R. Geoscience* **338,** 11–24 (2006).
3. Michard, A., Hoepffner, C., Soulaimani, A. & Baidder, L. The variscan belt. In *Continental Evolution: the Geology of Morocco* (eds. A. Michard, O. Saddiqi, A. Chalouan & D. Frizon de Lamotte) 65–132 (Lecture Notes in Earth Sciences Vol. 126, Springer, 2008).
4. Loi, A. *et al.* The Late Ordovician glacio-eustatic record from a highlatitude storm-dominated shelf succession: the Bou Ingarf section (Anti-Atlas, Southern Morocco). *Palaeogeogr. Palaeoclim. Palaeoeco.* **296,** 332–358 (2010).
5. Havlicek, V. Brachiopodes de l'Ordovicien du Maroc. *Notes Mém. Serv. Géol. Maroc* **230,** 1–135 (1971).
6. Sutcliffe, O.E., Harper, D.A.T., Aït Salem, A., Whittington, R.J. & Craig, J. The development of an atypical Hirnantian brachiopod fauna and the onset of glaciation in the Late Ordovician of Gondwana. *Trans. Roy. Soc. Edinburgh: Earth Sci.* **92,** 1–14 (2001).
7. Mergl, M. Faunal turnover near the Katian/Hirnantian boundary in the Prague Basin (Czech Republic). In *Ordovician of the World* (eds J.C. Gutiérrez-Marco, I. Rabano & D. Garcia-Bellido) 359–366 (Publ. Inst. Geol. Miner. Espana, Vol. 14, 2011).
8. Mitchell, C.E., Štorch, P., Holmden C., Melchin, M.J. & Gutiérrrez-Marco, J.C. New stable isotope data and fossils from the Hirnantian stage in Bohemia and Spain: Implications for correlation and paleoclimate. In *Ordovician of the World* (eds J.C. Gutiérrez-Marco, I. Rabano & D. Garcia-Bellido) 371–378 (Publ. Inst. Geol. Miner. Espana, Vol. 14, 2011).
9. Paris, F. The Ordovician chitinozoan biozones of the northern Gondwana Domain. *Rev. Palaeobot. Palynol.* **66,** 181–209 (1990).
10. Bourahrouh, A., Paris, F. & Elaouad-Debbaj, Z. Biostratigraphy, bodiversity and palaeoenvironments of the chitinozoans and associated palynomorphs from the Upper Ordovician of the Central Anti-Atlas, Morocco. *Rev. Palaeobot. Palynol.* **130,** 17–40 (2004).
11. Clerc, S. *et al*. Subglacial to proglacial depositional environments in an Ordovician glacial tunnel valley, Alnif, Morocco. *Palaeogeogr. Palaeoclim. Palaeoeco.* **370,** 127–144 (2013).
12. Ghienne, J.-F., Le Heron, D., Moreau, J., Denis, M. & Deynoux, M. The Late Ordovician glacial sedimentary system of the North Gondwana platform. In *Glacial Sedimentary Processes and Products* Vol. 39 (eds M. Hambrey *et al*.) 295–319 (International Association of Sedimentologists, Special Publication, Blackwells, 2007).
13. Le Heron, D. Late Ordovician glacial record of the Anti-Atlas, Morocco. *Sediment. Geol.* **201,** 93–110 (2007).
14. Le Heron D., Ghienne J.-F., El Houicha M., Khoukhi Y. & Rubino J.-L. Maximum extent of ice sheets in Morocco during the Late Ordovician glaciation. *Palaeogeogr. Palaeoclim. Palaeoeco.* **245,** 200–226 (2007).
15. Lüning, S., Craig, J., Loydell, D.K., Štorch, P. & Fitches, B. Lower Silurian 'hot shales' in North Africa and Arabia: regional distribution and depositional model. *Earth-Sci. Rev.* **49,** 121–200 (2000).
16. Nutz, A., Ghienne, J.-F. & Štorch, P. Circular, cryogenic structures from the Hirnantian deglaciation sequence (Anti-Atlas,Morocco). *J. Sediment. Res.* **83,** 115–131 (2013).
17. Long, D.G.F. Tempestite frequency curves: a key to Late Ordovician and Early Silurian subsidence, sea-level change, and orbital forcing in the Anticosti foreland basin, Quebec, Canada. *Can. J. Earth Sci.* **44,** 413–431 (2007).
18. Desrochers, A., Farley. C., Achab, A., Asselin, E. & Riva, J.F. A far-field record of the end Ordovician glaciation: The Ellis Bay Formation, Anticosti Island, Eastern Canada. *Palaeogeogr. Palaeoclim. Palaeoeco.* **296,** 248–263 (2010).

19. Achab, A., Asselin, E., Desrochers, A., Riva, J.F. & Farley, C. Chitinozoan biostratigraphy of a new Upper Ordovician stratigraphic framework for Anticosti Island, Canada. *Geol. Soc. Am. Bull.* **123,** 186–205 (2011).

20. Soufiane, A. & Achab, A. Chitinozoan zonation of the Late Ordovician and the Early Silurian of the Island of Anticosti, Quebec, Canada: *Rev. Palaeobot. Palynol.* **109,** 85-111 (2000).

21. Achab, A., Asselin, E., Desrochers, A. & Riva, J.F. The end-Ordovician chitinozoan zones of Anticosti Island, Québec: definition and stratigraphic position. *Rev. Palaeobot. Palynol.* **198,** 92–109 (2013).

22. Delabroye, A. *et al*. Phytoplankton dynamics across the Ordovician/Silurian boundary at low palaeolatitudes: Correlations with carbon isotopic and glacial events. *Palaeogeogr. Palaeoclim. Palaeoeco*. **312,** 79–97 (2011).

23. Copper, P. Reefs during the multiple crises towards the Ordovician-Silurian boundary: Anticosti Island, Eastern Canada, and worldwide. *Canad. J. Earth Sci.* **38,** 153–171 (2001).

24. Jin, J. & Copper, P. 2000. Late Ordovician and Early Silurian pentamerid brachiopods from Anticosti Island, Québec, Canada. *Palaeontograph. Canad.*, Vol. 18, 140pp.

25. Jin, J. & Copper, P. Origin and evolution of the Early Silurian (Rhuddanian) virgianid pentameride brachiopods — the extinction recovery fauna from Anticosti Island, eastern Canada. *Boll. Soc. Paleontol. Ital.* **49,** 1 –11 (2010).

26. Jin, J. & Copper, P. Parastrophinella (Brachiopoda): its paleogeographic significance at the Ordovician/Silurian boundary. *J. Paleontol.* **71,** 369–380 (1997).

27. Jin, J. & Copper, P. Response of brachiopod communities to environmental change during the Late Ordovician mass extinction interval, Anticosti Island, eastern Canada. *Fossils and Strata* **54,** 41–51 (2008).

28. Rongyu, L. & Copper, P. Early Silurian (Llandovery) orthide brachiopods from Anticosti Island, eastern Canada: the O/S extinction recovery fauna. *Spec. Pap. Palaeont.* **76,** 1–71 (2006).

29. Jin, J. & Zhan, R. B. Late Ordovician orthide and billingsellide brachiopods from Anticosti Island, Eastern Canada; diversity change through mass extinction. *National Research Council Research Press* (Ottawa, Canada, 2008).

30. Nestor, H., Copper, P. & Stock, C.W. Late Ordovician and Early Silurian stromatoporoid sponges from Anticosti Island, eastern Canada: crossing the O/S mass extinction boundary. *National Research Council Research Press* (Ottawa, 163 pp., 2010).

31. Melchin, M. J. Restudy of some Ordovician–Silurian boundary graptolites from Anticosti Island, Canada, and their biostratigraphic significance. *Lethaia* **41,** 55–62 (2008).

32. Ausich, W.I. & Copper, P. The Crinoidea of Anticosti Island (Late Ordovician and Early Silurian). *Palaeontograph. Canad.* Vol. 29 (2010).

33. Holland, C.H. & Copper, P. Ordovician and Silurian nautiloid cephalopods from Anticosti island: traject across the Ordovician-Silurian (O/S) mass extinction boundary. *Canad. J. Earth Sci.* **45,** 1015–1038 (2008).

34. Farley, C. *Sediment dynamics and stratigraphic architecture of a mixed carbonate-siliciclastic ramp: the upper ordovician (Hirnantian) Ellis Bay Formation, Anticosti Island, Québec, Canada*. Unpublished M.Sc. thesis, University of Ottawa, Canada (2008).

35. Wickson, S. *High-Resolution Carbon Isotope Stratigraphy of the Ordovician-Silurian Boundary on Anticosti Island, Quebec: Regional and Global Implications*. Unpublished M.Sc. thesis, University of Ottawa, Canada (2010).

36. Pinet, N. Hinterland-directed transtensional faulting at an orogen structural front: the example of the Cap-Chat Mélange, Quebec Appalachians. *Geol. Soc. Amer. Bull.* **123,** 2256–2265 (2011).

37. Ainsaar, L., *et al.* 2010. Middle and Upper Ordovician carbon isotope chemostratigraphy in Baltoscandia: A correlation standard and clues to environmental history. *Palaeogeogr. Palaeoclim. Palaeoeco.* **294,** 189–201 (2010).

38. Brenchley, P.J. *et al*. High-resolution stable isotope stratigraphy of Upper Ordovician sequences: Constraints on the timing of bioevents and environmental changes associated with mass extinction and glaciation. *Geol. Soc. Am. Bull.* **115,** 89–104 (2003).

39. Bergström, S.M., Saltzman, M.R. & Schmitz, B. First record of the Hirnantian (Upper Ordovician) $\delta^{13}C$ excursion in the North American Midcontinent and its regional implications. *Geol. Mag.* ***143,*** 657–678 (2006).

40. Bergström, S.M., Kleffner, M., Schmitz, B. & Cramer, B. Revision of the position of the Ordovician–Silurian boundary in southern Ontario: regional chronostratigraphic implications of à $\delta^{13}C$ chemostratigraphy of the Manitoulin Formation and associated strata. *Canad. J. Earth Sci.* **48,** 1447–1470 (2011).

41. Jones, D. S. *et al*. Terminal Ordovician carbon isotope stratigraphy and glacioeustatic sea-level change across Anticosti Island (Québec, Canada). *Geol. Soc. Amer. Bull.* **123,** 1645–1664 (2011).

42. Jervey, M.T. Quantitative geological modeling of siliciclastic rock sequences and their seismic expression. In *Sea Level Changes — An Integrated Approach* Vol. 42 (eds Wilgus, C.K. *et al*.) 47–69 (Society of Economic Paleontologists and Mineralogists, Special Publication, 1988).

43. Posamentier, H.W. & Vail, P.R. Eustatic controls on clastic deposition II – sequence and systems tract models. In *Sea-Level Changes – An Integrated Approach* Vol. 42 (eds C.K. Wilgus et al.) 125–154 (SEPM Special Publication, 1988).

44. Mountain, G.S. *et al.* The long-term stratigraphic record on continental margins - The long-term record. In *Continental Margin Sedimentation: From Sediment Transport to Sequence Stratigraph* Vol. 37 (eds C.A. Nittrouer *et al.)* 381-458 (International Association of Sedimentologists, Special Publication, Blackwells, 2007).

45. Meijer, X.D., Postma, G., Burrough, P.A. & De Boer P.L. Modelling the preservation of sedimentary deposits on passive continental margins during glacial-interglacial cycles. In *Analogue and Numerical Modelling of Sedimentary Systems: From Understanding to Prediction*. Vol. 40 (eds P. De Boer et al.) 223-238 (International Association of Sedimentologists, Special Publication, Blackwells, 2008).

46. Grader, G.W., Isaacson, P.E., Díaz-Martínez, E. & Pope, M.C. Pennsylvanian and Permian sequences in Bolivia: Direct responses to Gondwana glaciation. In *Resolving the Late Paleozoic Ice Age in Time and Space* Vol. 441 (eds C.R. Fielding, T.D. Frank & J.L. Isbell) 143–159 (Geological Society of America, Special Paper, 2008).

47. Heckel, P.H. Pennsylvanian cyclothems in Midcontinent North America as far-field effects of waxing and waning of Gondwana ice sheets. In *Resolving the Late Paleozoic Ice Age in Time and Space* Vol. 441 (eds C.R. Fielding, T.D. Frank & J.L. Isbell) 275–289 (Geological Society of America, Special Paper, 2008).

48. ten Brink, U.S. & Schneider, C. Glacial morphology and depositional sequences of the Antarctic continental shelf. *Geology* **23,** 580-584 (1995).

49. Pollard, D. & DeConto, R.M. A coupled ice-sheet/ice-shelf/sediment model applied to a marine-margin flowline: forced and unforced variations. In *Glacial Sedimentary Processes and Products* Vol. 39 (eds M. Hambrey *et al*.) 37–52 (International Association of Sedimentologists, Special Publication, Blackwells, 2007).

50. Bart, P.J. & Anderson J.B. Seismic expression of depositional sequences associated with expansion and contraction of ice sheets on the northwestern Antarctic Peninsula continental shelf. In *Geology of Siliciclastic Shelf Seas* Vol. 171 (eds M. de Batist & P. Jacobs) 171–186 (Geol. Soc. Spec. Publs, London, 1996).

51. Denis, M., Guiraud, M., Konaté, M. & Buoncristiani, J.-F. Subglacial deformation and water-pressure cycles as a key for understanding ice stream dynamics: evidence from the Late Ordovician succession of the Djado Basin (Niger). *Intern. J. Earth Sci.* **99,** 1399**–**1425 (2010).

52. Le Heron, D.P., Armstrong, H.A., Wilson, C., Howard, J.P. & Gindre, L. Glaciation and deglaciation of the Libyan Desert: The Late Ordovician record. *Sediment. Geol.* **223,** 100–125 (2010).

53. Helland-Hansen, W. & Hampson, G. Trajectory analysis: concepts and applications. *Basin Res.* **21,** 454–483 (2009).

54. Le Heron, D.P. & Craig, J. First-order reconstructions of a Late Ordovician Saharan ice sheet. *J. Geol. Soc.* **165,** 19–29 (2008).

55. Le Heron, D.P., Craig, J., Sutcliffe, O. & Whittington, R. Late Ordovician glaciogenic reservoir heterogeneity: an example from the Murzuq Basin Libya. *Marine Petrol. Geol.* **23,** 655–677 (2006)

56. Videt. B. et al. (2010) Biostratigraphical calibration of the third-order Ordovician sequences on the northern Gondwana platform. *Palaeogeogr. Palaeoclim. Palaeoeco.* **298,** 359–375 (2010).

57. Girard, F., Ghienne, J.-F. & Rubino, J.-L. Occurrence of hyperpycnal flows and hybrid event beds related to glacial outburst évents in a Late Ordovician proglacial delta (Murzuq Basin, SW Libya). *J. Sediment. Res.* **82,** 688–708 (2012).

58. Ghienne, J.-F., Moreau, J., Degermann, L. & Rubino, J.-L. Lower Palaeozoic unconformities in an intracratonic platform setting: glacial erosion versustectonics in the eastern Murzuq Basin (southern Libya). *Intern. J. Earth Sci.* **102,** 455–482 (2013).

59. Deschamps, R., Eschard, R. & Rousse, S. Architecture of Late Ordovician glacial valleys in the Tassili N'Ajjer area (Algeria). *Sediment. Geol.* **289,** 124–147 (2013).

60. Mackenzie, F.T. & Lerman, A. *Carbon in the geobiosphere: in Earth's Outer Shell* (Springer, London, 2006).

61. Cramer, B. & Saltzman, M.R. Sequestration of 12C in the deep ocean during the early Wenlock (Silurian) positive carbon isotope excursion. *Palaeogeogr. Palaeoclim. Palaeoeco.* **219,** 333–349 (2005).

62. Cramer, B.S., & Saltzman, M.R. Fluctuations in epeiric sea carbonate production during Silurian positive carbon isotope excursions: A review of proposed paleoceanographic models. *Palaeogeogr. Palaeoclim. Palaeoeco.* **245,** 37–45 (2007).

63. de Boer, P.L. & Alexandre, J.T. Orbitally forced sedimentary rhythms in the stratigraphic record: is there room for tidal forcing? *Sedimentology* **59,** 379–392 (2012).

64. Brenchley, P.J. *et al*. Bathymetric and isotopic evidence for a shortlived Late Ordovician glaciation in a greenhouse period. *Geology* **22,** 295–298 (1994).

65. Kump, L.R. *et al*. A weathering hypothesis for glaciation at high atmospheric pCO_2 during the Late Ordovician. *Palaeogeogr. Palaeoclim. Palaeoeco* **152,** 173–187 (1999).

66. Melchin, M.J. & Holmden, C. Carbon isotope chemostratigraphy in Arctic Canada: Sea-level forcing of carbonate platform weathering and implications for Hirnantian global correlation. *Palaeogeogr. Palaeoclim. Palaeoeco.* **234,** 186–200 (2006).

67. LaPorte, D.F. *et al*. Local and global perspectives on carbon and nitrogen cycling during the Hirnantian glaciation. *Palaeogeogr. Palaeoclim. Palaeoeco* **276,** 182–195 (2009).

68. Veizer, J. *et al.* $^{87}Sr/^{86}Sr$, $\delta^{13}C$ and $\delta^{18}O$ evolution of Phanerozoic seawater. *Chem. Geol.* **161,** 59–88 (1999).

69. Bickert, T., Pätzold, J., Samtleben, C. & Munnecke, A. Paleoenvironmental changes in the Silurian indicated by stable isotopes in brachiopod shells from Gotland, Sweden. *Geochim. Cosmochim. Acta* 61, 2717–2730 (1997).

70. Jeppson, L. & Calner, M. The Silurian Mulde Event and a scenario for a secundo-secundo events. *Trans. Roy. Soc. Edinburgh, Earth Sci.* **93,** 135–154 (2003).

71. Munnecke, A., Samtleben, C. & Bickert, T. The Ireveken event in the lower Silurian of Gotland, Sweden — relation to similar Palaeozoic and Proterozoic events. *Palaeogeogr. Palaeoclim. Palaeoeco.* **195,** 99–124 (2003).